Article

Neuron

Synaptojanin and Endophilin Mediate Neck Formation during Ultrafast Endocytosis

Graphical Abstract

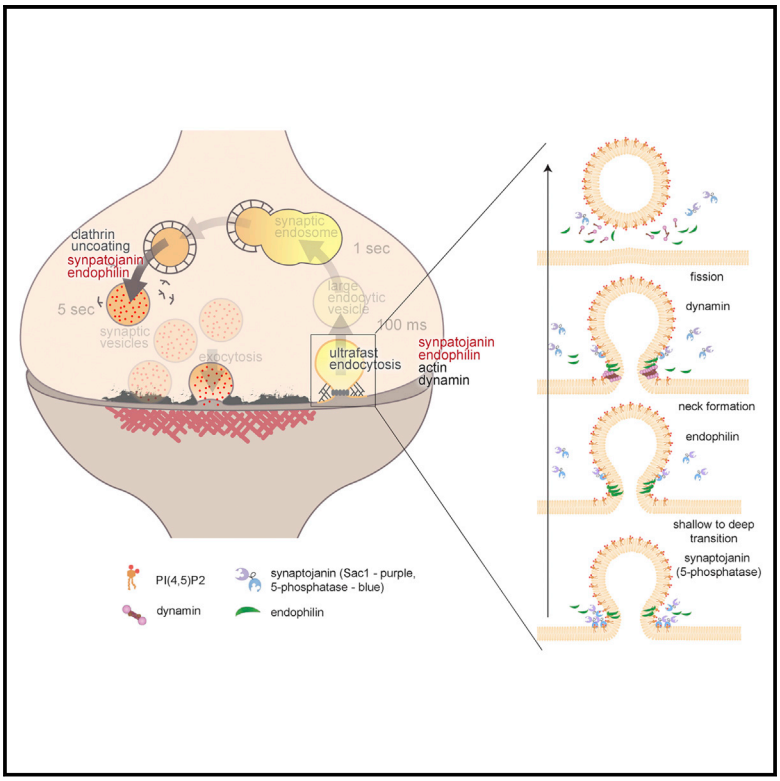

Highlights

- Synaptojanin and endophilin accelerate ultrafast endocytosis
- Neck formation requires endophilin and the 5-phosphatase activity of synaptojanin
- Synaptic vesicles still form from synaptic endosomes in absence of these proteins
- Endophilin and 4- and 5-phosphatase are required for clathrin uncoating

Authors

Shigeki Watanabe, Lauren Elizabeth Mamer, Sumana Raychaudhuri, ..., Ira Milosevic, Christian Rosenmund, Erik M. Jorgensen

Correspondence

shigeki.watanabe@jhmi.edu (S.W.), christian.rosenmund@charite.de (C.R.), jorgensen@biology.utah.edu (E.M.J.)

In Brief

Ultrafast endocytosis is a distinct form of synaptic vesicle recovery occurring within milliseconds of vesicle fusion. Using flash-and-freeze electron microscopy, Watanabe et al. demonstrate dual roles for synaptojanin and endophilin in membrane remodeling and clathrin uncoating on rapid timescales during ultrafast endocytosis.

Watanabe et al., 2018, Neuron *98*, 1184–1197
June 27, 2018
https://doi.org/10.1016/j.neuron.2018.06.005

CellPress

CellPress

Neuron
Article

Synaptojanin and Endophilin Mediate Neck Formation during Ultrafast Endocytosis

Shigeki Watanabe,[1,2,3,8,9,*] Lauren Elizabeth Mamer,[1,4,8] Sumana Raychaudhuri,[2] Delgermaa Luvsanjav,[2] Julia Eisen,[7] Thorsten Trimbuch,[1] Berit Söhl-Kielczynski,[1] Pascal Fenske,[1] Ira Milosevic,[6] Christian Rosenmund,[1,9,*] and Erik M. Jorgensen[1,5,9,10,*]

[1]Department of Neurophysiology, NeuroCure Cluster of Excellence, Charité-Universitätsmedizin Berlin, Berlin, Germany
[2]Department of Cell Biology, Johns Hopkins University, School of Medicine, Baltimore, MD 21205, USA
[3]Solomon H. Snyder Department of Neuroscience, Johns Hopkins University, School of Medicine, Baltimore, MD 21205, USA
[4]The Ohio State University College of Medicine, The Ohio State University, Columbus, OH 43210, USA
[5]Department of Biology and Howard Hughes Medical Institute, University of Utah, Salt Lake City, UT 84112-0840, USA
[6]Synaptic Vesicle Dynamics, European Neuroscience Institute, University Medical Center Göttingen, 37077 Göttingen, Germany
[7]Barnard College of Columbia University, New York, NY, USA
[8]These authors contributed equally
[9]Senior author
[10]Lead Contact
*Correspondence: shigeki.watanabe@jhmi.edu (S.W.), christian.rosenmund@charite.de (C.R.), jorgensen@biology.utah.edu (E.M.J.)
https://doi.org/10.1016/j.neuron.2018.06.005

SUMMARY

Ultrafast endocytosis generates vesicles from the plasma membrane as quickly as 50 ms in hippocampal neurons following synaptic vesicle fusion. The molecular mechanism underlying the rapid maturation of these endocytic pits is not known. Here we demonstrate that synaptojanin-1, and its partner endophilin-A, function in ultrafast endocytosis. In the absence of synaptojanin or endophilin, the membrane is rapidly invaginated, but pits do not become constricted at the base. The 5-phosphatase activity of synaptojanin is involved in formation of the neck, but 4-phosphatase is not required. Nevertheless, these pits are eventually cleaved into vesicles; within a 30-s interval, synaptic endosomes form and are resolved by clathrin-mediated budding. Then synaptojanin and endophilin function at a second step to aid with the removal of clathrin coats from the regenerated vesicles. These data together suggest that synaptojanin and endophilin can mediate membrane remodeling on a millisecond timescale during ultrafast endocytosis.

INTRODUCTION

Although classic ultrastructural studies suggest that synaptic vesicles are recycled by clathrin-mediated endocytosis (Heuser and Reese, 1973; Miller and Heuser, 1984), recent morphological studies indicate that synaptic vesicle membranes in at least several synaptic types are recycled by ultrafast endocytosis (Watanabe et al., 2013a, 2013b). Optogenetic stimulation followed by rapid freezing, called "flash-and-freeze," can capture the progress of endocytosis with millisecond temporal resolution in electron micrographs. Ultrafast endocytosis can recover membrane as rapidly as 30–300 ms after stimulation at the lateral edge of active zones. This rapid process of endocytosis does not require clathrin, but it is only observed at physiological temperatures; at room temperature, clathrin-mediated endocytosis prevails (Watanabe et al., 2014). Ultrafast endocytosis can also be observed in low-noise capacitance measurements in cerebellar and hippocampal mossy fiber synapses (Delvendahl et al., 2016). After a 10-Hz stimulation, endocytosis slows to a fast time constant of 760 ms and a slow time constant of 26 s even at 37°C when measured using rapid quenching (Soykan et al., 2017). After ultrafast endocytosis, the ~80-nm vesicles translocate to the distal edge of the synapse (Watanabe et al., 2014). Because the fluid phase marker ferritin is found in a large endosome-like structure (~120 nm), either endocytic vesicles fuse together via homotypic fusion or fuse to a pre-existing organelle to form the synaptic endosome. Clathrin-coated vesicles then bud off from the synaptic endosomes, and synaptic vesicles are recovered by shedding these clathrin coats (Watanabe et al., 2014). Genetic knockout of AP2 results in the accumulation of endosomes in these terminals (Gu et al., 2008, 2013; Kononenko et al., 2014), further supporting the idea that clathrin functions at endosomes for vesicle regeneration. These data suggest that action potential-induced vesicle endocytosis is fast and clathrin-independent.

Despite its rapid timescale, the coordinated actions of multiple proteins are likely required to generate vesicles via ultrafast endocytosis. Membrane invagination requires polymerized actin. Latrunculin-A sequesters monomeric G-actin and inhibits polymerization; when applied to mouse hippocampal neurons, membrane buckling fails completely (Watanabe et al., 2013b). Vesicle scission is likely mediated by dynamin because temperature-sensitive mutants or pharmacological inhibition of dynamin traps endocytic vesicles at the plasma membrane (Watanabe et al., 2013a, 2013b). However, apart from actin and dynamin, the protein machinery required for ultrafast endocytosis is not understood.

Two proteins thought to function with dynamin are endophilin and synaptojanin. Endophilin-A (hereafter called endophilin) is composed of a Bin Amphiphysin, Rvs (BAR) domain and an SH3 domain (de Heuvel et al., 1997; Ringstad et al., 1997, 2001). BAR domains can bind and tubulate membranes *in vitro* (Farsad et al., 2001; Frost et al., 2009; Peter et al., 2004), and the SH3 domain binds the proline-rich domain of dynamin (Shupliakov et al., 1997). Perturbation studies indicate that endophilin is required for endocytosis in lampreys (Gad et al., 2000), flies (Verstreken et al., 2002), worms (Schuske et al., 2003), mice (Milosevic et al., 2011), and yeast (Kaksonen et al., 2005). In studies of synapses in endophilin mutants, there was a depletion of synaptic vesicles and an accumulation of coated vesicles. Furthermore, endophilin functions in clathrin-independent endocytosis to mediate rapid internalization of receptors from the surface (Boucrot et al., 2015). Thus, it is a particularly interesting candidate to investigate in the context of ultrafast endocytosis, in which the steps of membrane endocytosis and clathrin-mediated vesicle formation are separated in both time and space (Watanabe et al., 2014).

The SH3 domain of endophilin also binds the proline-rich domain of synaptojanin-1 (hereafter called synaptojanin) (Micheva et al., 1997; Verstreken et al., 2003). Genetic studies indicate that synaptojanin plays a role in endocytosis in mice (Cremona et al., 1999; Milosevic et al., 2011), worms (Harris et al., 2000), flies (Dickman et al., 2005; Verstreken et al., 2003), and yeast (Stefan et al., 2005). In studies of synapses, synaptojanin mutants exhibit a decrease in total synaptic vesicle numbers and an accumulation of clathrin-coated vesicles, like in endophilin mutants. Endophilin and synaptojanin work cooperatively in endocytosis and subsequent uncoating of clathrin because double mutants are identical to single mutants (Schuske et al., 2003; Verstreken et al., 2003). Synaptojanin contains two phosphoinositide phosphatase domains (McPherson et al., 1996): a SacI-like phosphatase that acts on the 3 and 4 positions on the inositol ring and 5-phosphatase, which acts on the 5 position on the inositol ring (Guo et al., 1999; Nemoto et al., 2001). Both domains are critical for endocytosis and clathrin uncoating during clathrin-mediated endocytosis (Cao et al., 2017; Mani et al., 2007).

Here we use flash-and-freeze electron microscopy in mouse hippocampal neurons to examine the roles of synaptojanin and endophilin in ultrafast endocytosis. In both mutants, the endocytic membrane is stalled at the plasma membrane for an extended period of time (1–10 s) but is resolved by 30 s. In both endophilin and synaptojanin mutants, synaptic vesicles still form by clathrin-mediated budding from synaptic endosomes, but removal of clathrin from these vesicles is delayed. The failure to fully acidify synaptic vesicles in these mutants suggests that acidification of synaptic vesicles takes place after clathrin-coats are removed. Taken together, these data suggest that endophilin and synaptojanin play dual roles during synaptic vesicle recycling: neck formation during ultrafast endocytosis and clathrin uncoating following regeneration of synaptic vesicles from endosomes.

RESULTS

Synaptojanin Is Required for Rapid Vesicle Formation

Mice with null mutations in synaptojanin die perinatally (Cremona et al., 1999). To determine the role of synaptojanin in ultrafast endocytosis, we cultured hippocampal neurons from synaptojanin knockout animals (*Synj1*$^{-/-}$; Cremona et al., 1999) and wild-type animals (*Synj1*$^{+/+}$) prepared from the same litters (n = 3 cultures). Cultures were infected using a lentivirus expressing a variant of channelrhodopsin, ChetaTC (Berndt et al., 2011; Gunaydin et al., 2010). Cultured neurons were exposed to a 10-ms pulse of light, and the subsequent membrane dynamics were captured by freezing the neurons at defined time points from 30 ms to 30 s after stimulation (37°C, 4 mM Ca^{2+}).

In wild-type neurons, endocytic structures were observed at the lateral edge of the active zone 100 ms after stimulation in 27% of the synapses (58 of 215 synapses; Figures 1A and S1A), consistent with previous measures of ultrafast endocytosis (Watanabe et al., 2013b). At this time, endocytic pits were typically deeply invaginated (pit depth, 71.0 ± 1.8 nm; 25 of 58 endocytic structures; Figure 1E) or fully internalized as large endocytic vesicles (diameter, 66.3 ± 1.9 nm; 33 of 58 endocytic structures; Figures 1A, 1C, 1G, and S1A). 300 ms after stimulation, endocytic pits were almost completely absent (endocytic pits, 3 of 208 synapses), and only large endocytic vesicles were present at endocytic sites (large endocytic vesicles near the active zone, 14 of 208 synapses; Figure 1C), suggesting that ultrafast endocytosis is largely complete by this time point. These endocytic vesicles were then translocated to the center of the bouton to fuse and become synaptic endosomes, which are plentiful from ~300 ms to 1 s (300 ms, 56 of 208 synapses; 1 s, 57 of 210 synapses; and 3 s, 38 of 210 synapses). These synaptic endosomes were resolved by clathrin-mediated budding into coated vesicles starting at ~3 s post-stimulation (Figures 1A, 1C, and S1A).

In synaptojanin mutant neurons, endocytic pits also formed 100 ms after stimulation and were localized at the lateral edge of the active zone in 15% of the synapses (43 of 287 synapses; Figures 1B, 1D, and S1B). However, fully resolved large endocytic vesicles were rarely observed at these sites (2 of 43 endocytic structures; Figure 1G), and unresolved endocytic pits remained at the plasma membrane for 1–10 s (Figure 1D). These endocytic pits were slightly shallower and wider than in wild-type neurons (Figures 1E and 1F; pit depth: *Synj1*$^{-/-}$, 62.4 ± 2.8 nm, wild-type [WT], 71.0 ± 1.8 nm, $p < 0.05$; pit width: *Synj1*$^{-/-}$, 126.1 ± 5.4 nm, n = 44 pits; wild-type 111.7 ± 9.2 nm, n = 25 pits; p = 0.19). Moreover, in the wild-type neurons, necks narrowed to 0 nm; in synaptojanin mutants, the neck was never narrower than 38.3 nm. These data suggest that formation of a neck during vesicle invagination requires synaptojanin.

The Membrane Is Ultimately Internalized In Synaptojanin Mutants

Do the pits eventually resolve into endocytic vesicles or do they collapse back into the plasma membrane? Large endocytic vesicles were occasionally observed at synaptojanin mutant synapses between 100 ms and 10 s (17 of 1,034 synapses; Figure 1D). Because large endocytic vesicles are very transient (~200 ms), they can only be observed immediately after their formation. The temporal resolution of our ultrastructural analysis is too coarse after 1 s to reliably capture such transient structures. However, the eventual appearance of synaptic endosomes and coated vesicles, albeit with a delay, suggests that endocytosis proceeds in synaptojanin mutants (Figures 1B, 1D, and S1B).

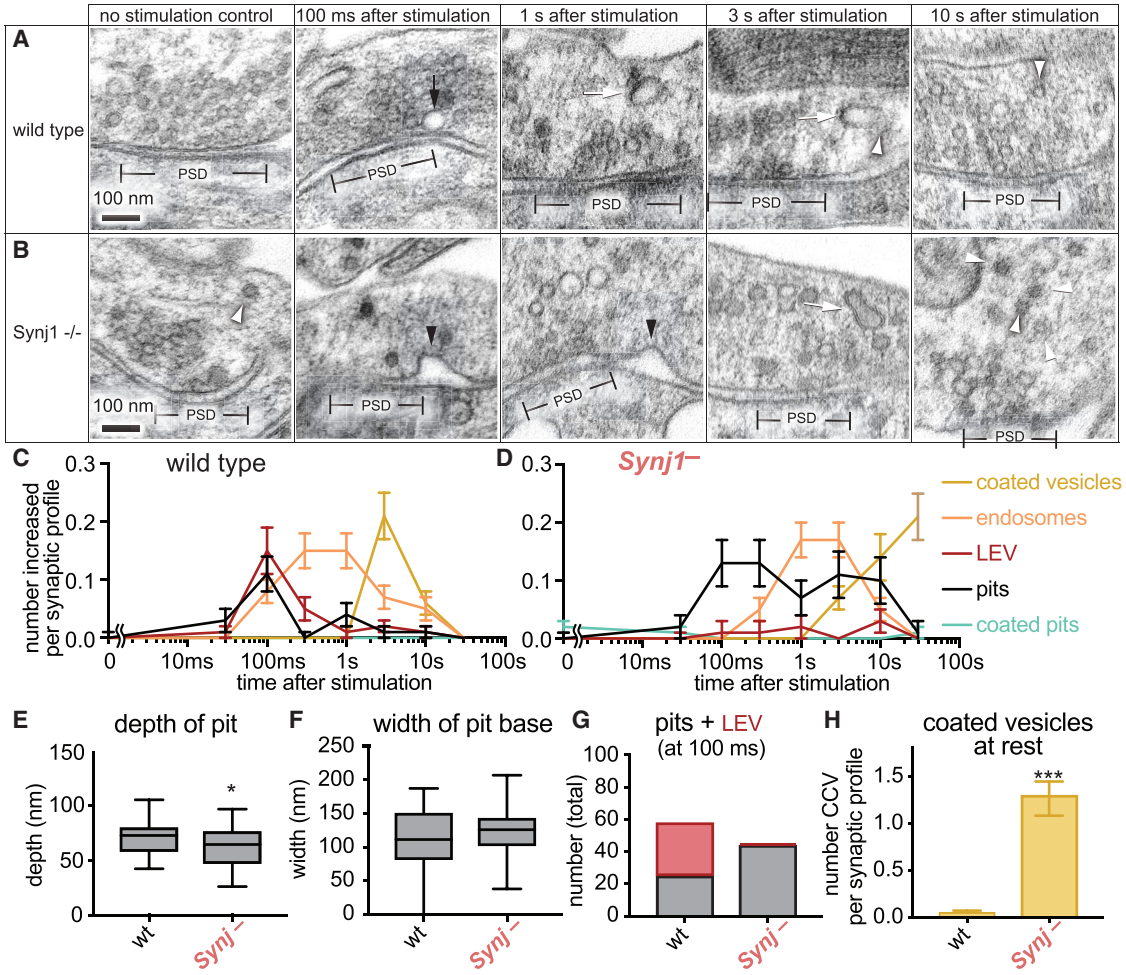

Figure 1. Synaptojanin Is Necessary for Rapid Formation of Ultrafast Endocytic Vesicles and for Clathrin Uncoating

(A and B) Example electron micrographs representing endocytic intermediates at the indicated time points in wild-type neurons (A) and *Synj1*$^{-/-}$ neurons (B). Black arrowheads, endocytic invaginations; black arrows, large endocytic vesicles (LEVs); white arrows, endosomes; white arrowheads, clathrin-coated vesicles. Large endocytic vesicles are large endocytic vesicles located within 50 nm of both the plasma membrane and the edge of the active zone. Note that endocytic invaginations and clathrin-coated vesicles persist longer in *Synj1*$^{-/-}$ neurons.

(C and D) Plots showing the increase in the number of each endocytic structure per synaptic profile after a single stimulus in wild-type neurons (C) and *Synj1*$^{-/-}$ neurons (D).

(E and F) Plots showing the height (E) and width (F) of endocytic invaginations at 100-ms time points.

(G) Total number of endocytic pits and large endocytic vesicles found at the 100-ms time point in the respective genotypes.

(H) Number of clathrin-coated vesicles in the resting terminals. The mean and SEM are shown in each graph. PSD, post-synaptic density. n = 3 cultures. See Quantification and Statistical Analysis for the n values and detailed numbers for each time point. See Figure S1 for additional images. *$p < 0.05$, ***$p < 0.001$. Wild-type neurons are from *Synj1*$^{+/+}$ littermates in all cases.

To track endocytic structures, we applied cationized ferritin particles in the external solution and performed flash-and-freeze experiments (single stimulus, 37°C, 4 mM Ca^{2+}). In wild-type neurons, ferritin particles are in endocytic vesicles at 100 ms (Watanabe et al., 2014), endosomes at 1 s, and clathrin-coated vesicles at 3 s (Figures 2A, 2B, and S2A). Thus, the presence of ferritin particles in large endocytic vesicles or synaptic endosomes by 1 s poststimulation suggests successful completion of ultrafast endocytosis.

In synaptojanin mutant neurons, ferritin particles are almost exclusively found in endocytic pits at 1 s (Figures 2C, 2D, and S2B). At 3 s, a decline in endocytic pits at the plasma membrane is observed in synaptojanin mutants, and this decrease is correlated with a concomitant increase in ferritin in organelles within the bouton (Figure 2D). These organelles include large endocytic vesicles (10 of 170 synapses, 60–80 nm), but they are not close to the plasma membrane (233.2 ± 26.3 nm on average), suggesting that they are rapidly trafficked away from the endocytic zone. Ferritin is also observed in large synaptic endosomes (>100 nm) at 3 s and in a few clathrin-coated vesicles that have budded from the synaptic endosomes. By contrast, clathrin-coated pits are not observed on the plasma membrane (Figure 2D), suggesting that clathrin-mediated endocytosis is not compensating for defective ultrafast endocytosis in synaptojanin mutants. These

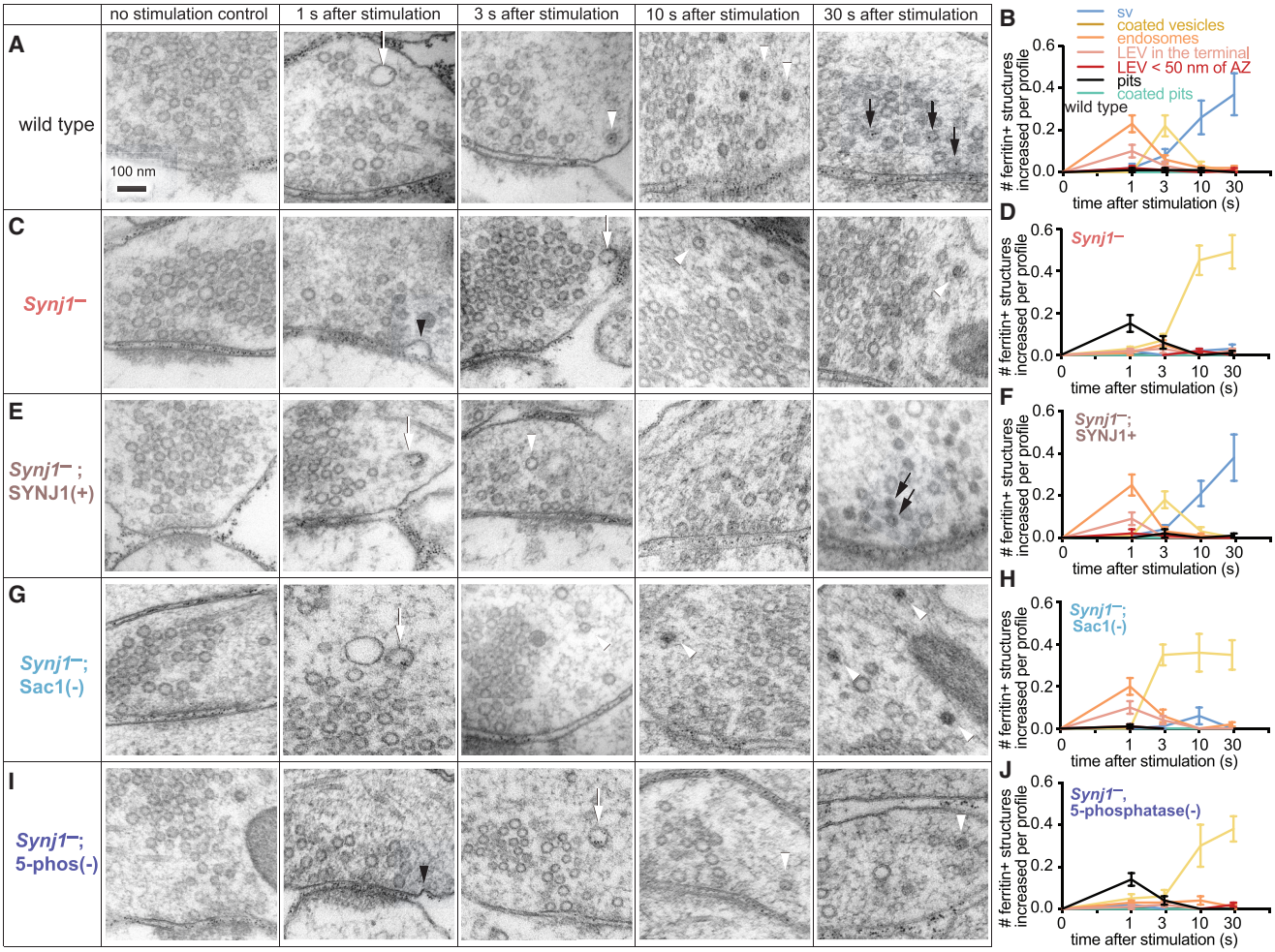

Figure 2. Synaptojanin 5-Phosphatase Is Necessary for the Efficient Formation of Endocytic Vesicles

(A, C, E, G, and I) Example micrographs showing ferritin-containing endocytic structures at the indicated time points in *Synj1*$^{+/+}$ neurons (A), *Synj1*$^{-/-}$ neurons (C), *Synj1*$^{-/-}$, SYNJ1 (145-kDa isoform) neurons (E), *Synj1*$^{-/-}$, SYNJ1^{C383S} (145-kDa isoform) neurons (G), and *Synj1*$^{-/-}$, SYNJ1^{D730A} (145-kDa isoform) neurons (I). Black arrowheads, endocytic invaginations; white arrows, large endocytic vesicles and endosomes; white arrowheads, clathrin-coated vesicles; black arrows, synaptic vesicles. Note that the endocytic defect can be rescued with Sac1-dead but not with 5-phosphatase-dead synaptojanin.

(B, D, F, H, and J) Plots showing increases in the number of each endocytic structures per synaptic profile after a single stimulus in *Synj1*$^{+/+}$ neurons (B), *Synj1*$^{-/-}$ neurons (D), *Synj1*$^{-/-}$, SYNJ1 (145-kDa isoform) neurons (F), *Synj1*$^{-/-}$, SYNJ1^{C383S} (145-kDa isoform) neurons (H), and *Synj1*$^{-/-}$, SYNJ1^{D730A} (145-kDa isoform) neurons (J). "LEV within 50 nm of AZ" represents ferritin-positive large endocytic vesicles that are present within 50 nm both from the plasma membrane and from the edge of the active zone. These are likely nascent endocytic vesicles. "LEV in the terminal" represents ferritin-positive large endocytic vesicles that are present elsewhere in the terminal.

The mean and SEM are shown in each graph. n = 2 cultures. See Quantification and Statistical Analysis section for the detailed n values and numbers for each time point. See Figure S2 for additional images.

results suggest that ultrafast endocytosis is slowed but not blocked in the absence of synaptojanin and that, eventually, vesicles are regenerated by clathrin-mediated budding from the synaptic endosome.

Synaptojanin Is Required for Removing Clathrin from Coated Vesicles

There is a second requirement for synaptojanin during uncoating of vesicles. In wild-type synapses, clathrin-coated vesicles appear 3 s after stimulation and are largely gone by 10 s (Figures 1A and 1C). Synaptic endosomes exhibit a precursor-product relationship with coated vesicles because the decrease in synaptic endosomes with ferritin is associated with a concomitant increase in coated vesicles containing ferritin (Figures 2A and 2B). By contrast, in synaptojanin mutants, a high abundance of clathrin-coated vesicles is observed even in unstimulated synapses (Figure 1H). After stimulation, additional clathrin-coated vesicles began accumulating at 3 s and continued to increase at 30 s (Figures 1B, 1D, 2C, and 2D). Previous studies have demonstrated that coated vesicles accumulate in synaptojanin mutants at rest (Cremona et al., 1999; Harris et al., 2000; Verstreken et al., 2003). Our data

extend these findings and demonstrate that synaptojanin is required for the uncoating of synaptic vesicles following ultrafast endocytosis after an acute stimulus.

Differential Requirements for 5-Phosphatase and 4-Phosphatase Activities

Synaptojanin contains two phosphoinositide phosphatase domains. The Sac1 phosphatase domain cleaves the 4-phosphate from phosphatidylinositol 4-phosphate (PI4P) and the 3-phosphate from phosphatidylinositol 3-phosphate (PI3P) and phosphatidylinositol (3,5)-bisphosphate ($PI(3,5)P_2$), and the 5-phosphatase domain cleaves the 5-phosphate from phosphatidylinositol (4,5)-bisphosphate ($PI(4,5)P_2$) and phosphatidylinositol (3,4,5)-trisphosphate ($PI(3,4,5)P_3$) (Guo et al., 1999; Nemoto et al., 2001). To test whether the activities of these domains are required for ultrafast endocytosis, we generated full-length rescue constructs in the 145-kD isoform with either wild-type or mutant versions of each of the phosphatase active sites, as described previously (Mani et al., 2007). Synaptojanin mutant neurons were infected with these constructs (Figure S2F) and subjected to flash-and-freeze electron microscopy (single stimulus, 37°C, 4 mM Ca^{2+}). In all cases, expression of these constructs did not alter excitatory postsynaptic currents (EPSCs) (Figure S2G). Expression of full-length synaptojanin completely rescues the endocytic defect observed in synaptojanin-null mutants (Figures 2E, 2F, and S2C). The Sac1-dead synaptojanin ($SYNJ1^{C383S}$) rescued the endocytic defect, suggesting that Sac1 activity is not required for ultrafast endocytosis (Figures 2G, 2H, and S2D). By contrast, the 5-phosphatase-dead synaptojanin ($SYNJ1^{D730A}$) failed to rescue the defect in ultrafast endocytosis (Figures 2I, 2J, and S2E), suggesting that ultrafast endocytosis requires removal of the 5-phosphate group from the inositol ring of $PI(4,5)P_2$. Previous experiments have suggested that clathrin-mediated endocytosis at synaptic terminals requires the 5-phosphatase activity of synaptojanin (Dong et al., 2015; Mani et al., 2007). Our results indicate that the 5-phosphatase is required for ultrafast endocytosis.

Formation and resolution of the synaptic endosome into clathrin-coated vesicles appears to be normal in synaptojanin mutants, but removing the clathrin coat requires the activity of both phosphatases. In Sac1-dead neurons, vesicles with ferritin all retained their coats after budding from endosomes (Figures 2E–2H, and S2D); thus, the 4-phosphatase is required to uncoat vesicles generated from the synaptic endosome after acute stimulation. These data are consistent with the chronic accumulation of coated vesicles observed in a mutant lacking function in the Sac1 domain (Cao et al., 2017). In 5-phosphatase-dead neurons, all synaptic vesicle-sized structures with ferritin also retained coats, suggesting a profound defect in uncoating in these synapses (Figures 2I, 2J, 3H, and S2E). Together, these data suggest that both the 4-phosphatase and 5-phosphatase are required for uncoating vesicles. However, it is possible that only the 4-phosphatase acts during uncoating and that the defect observed in the 5-phosphatase mutant is indirect. Because the Sac1 phosphatase cannot cleave the 4-phosphate in the presence of the 5-phosphate (Guo et al., 1999), then failure to cleave the 5-phosphate during endocytosis would block Sac1 activity during uncoating.

Acidification of Vesicles after Clathrin Uncoating

To determine endocytic rates of synaptic vesicle proteins rather than membranes, we assayed quenching of pHluorin-tagged synaptophysin. After synaptic vesicles are regenerated, they are acidified by the vacuolar ATPase, and fluorescence is quenched (Balaji and Ryan, 2007; Granseth et al., 2006; Miesenböck et al., 1998). These assays are performed using high-frequency stimulation using 10–100 action potentials to obtain a significant fraction of vesicle proteins on the surface. Similar stimulation protocols induce multiple rounds of ultrafast endocytosis (Watanabe et al., 2013b). However, in the pHluorin assay, the decay in fluorescence depends on the rate of synaptophysin translocation to an endocytic site, the speed of endocytosis, and the rate of acidification. Because decay in fluorescence is an indirect measure of endocytosis, speeds measured by electron microscopy will be faster than observed for fluorescence decay.

Cultured neurons expressing synaptophysin-pHluorin (sypHy) were perfused with extracellular solution at 35°C and stimulated with either 10 action potentials at 20 Hz (0.5 s) or 75 action potentials at 10 Hz (7.5 s). The time constant for fluorescence decay in wild-type neurons following 10 action potentials was ~8 s (20 Hz at 35°C) (Figures 3A and 3B). Similarly, the time constant for fluorescence decay following 75 action potentials (10 Hz at 35°C) was ~9 s in the wild-type (Figures 3C and 3D). However, 75 action potentials increased the signal-to-noise ratio substantially compared with 10 action potentials; this protocol was used thereafter. Endocytosis of proteins is greatly accelerated at physiological temperatures (Balaji et al., 2008; Soykan et al., 2017). We also note that the time constant for fluorescence decay accelerates from ~20 s at 22°C to ~9 s at 35°C (Figure S2H), similar in magnitude to previous studies.

pHluorin quenching rates were determined for the synaptojanin mutant strain-expressing variants. Quenching of pHluorin is strongly defective in synaptojanin-null synapses (Figure 3A), consistent with previous experiments (Mani et al., 2007). Expression of the wild-type synaptojanin protein in *Synj1*$^{-}$ neurons fully rescued acidification (Figures 3E and 3H; 75 action potentials, wild-type τ = 9 s, *Synj1*$^{-}$ τ = 49 s, *Synj1*$^{-}$ SYNJ1+ τ = 7 s, $p < 0.01$; Figure 3D; 10 action potentials, wild-type τ = 8 s, *Synj1*$^{-}$ τ = 48 s, *Synj1*$^{-}$ SYNJ1+ τ = 13 s, $p < 0.05$). Expression of the 5-phosphatase(−) variant did not rescue quenching in the synaptojanin mutant synapses (Figures 3G and 3H; 75 action potentials, τ = 36 s, $p > 0.05$; Figure 3D; 10 action potentials, τ = 73 s). Expression of the Sac1(−) 5-phos(+) variant exhibited a slight acceleration in quenching relative to the null mutant (Figures 3D, 3F, 3H, and 3I), likely because of the presence of normal rates of ultrafast endocytosis, but this was not reflected in a significant improvement in the time constant for quenching (Figure 3D; 75 action potentials, wild-type 9 s, *Synj1*$^{-}$ 49 s, *Synj1*$^{-}$ +Sac1(−) 36 s, $p > 0.05$; Figure 3B; 10 action potentials, wild-type 8 s, *Synj1*$^{-}$ 48 s, *Synj1*$^{-}$ +Sac1(−) 19 s, not significant). Notably, in the wild-type, fluorescence reaches baseline in 40 s (~pH 5.5 for synaptic vesicles), but in the synaptojanin mutants, fluorescence never reached baseline in the course of the experiment, and only ~50% of the fluorescence was quenched at 30 s (Figure 3I). In the flash-and-freeze experiments, mutation of either the Sac1 domain or the 5-phosphatase domain exhibited a defect in vesicle uncoating (Figures 2G-2J, S2D and S2E, and

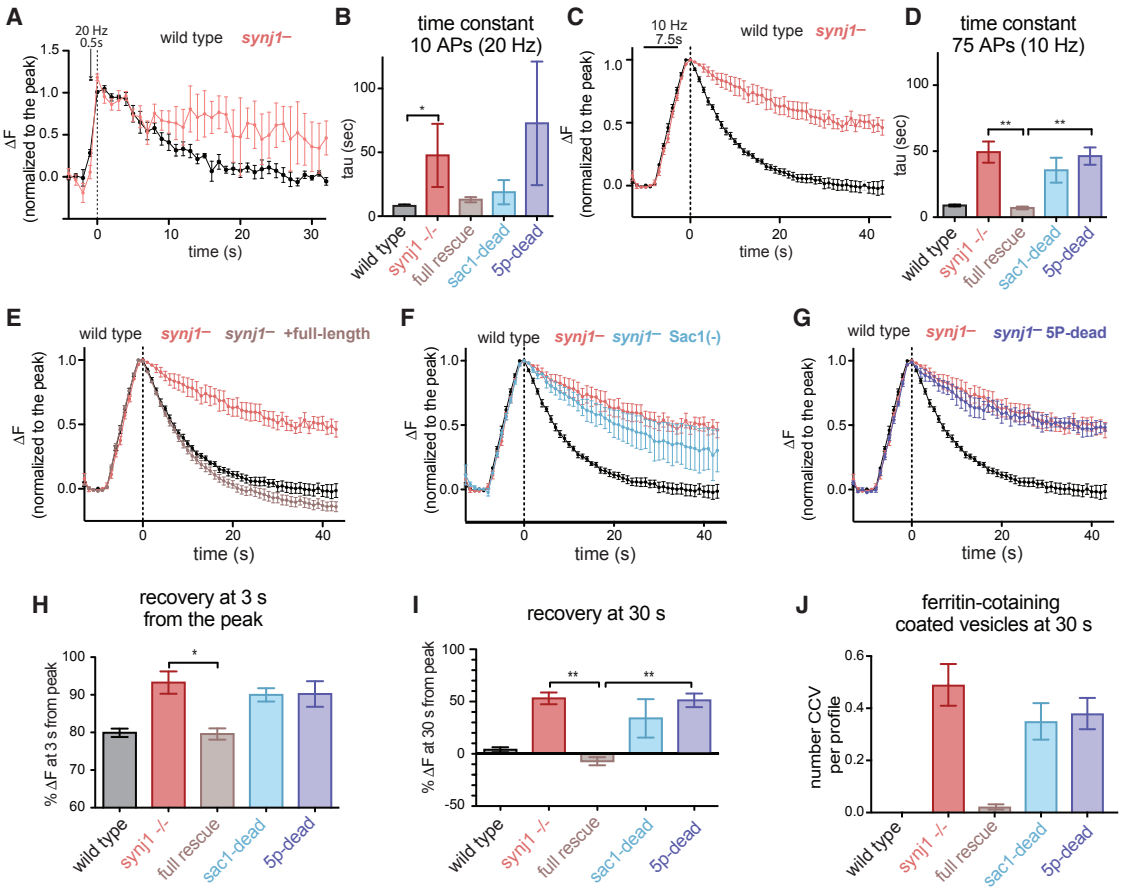

Figure 3. Both Sac1 and 5-Phosphatase Activities of Synaptojanin Are Required for Synaptic Vesicle Acidification Rates at 35°C

(A and C) Plots showing average responses of synaptophysin-pHluorin in *Synj1*$^{+/+}$ neurons (black) and *Synj1*$^{-/-}$ neurons (red) to 20 Hz, 10 stimuli (A) and to 10 Hz, 75 stimuli (C).

(B and D) The time constant for fluorescence recovery following 20 Hz, 10 stimuli (B) and 10 Hz, 75 stimuli (D). The time constants were obtained by fitting each pHluorin trace to a single exponential decay. The time constant is displayed as mean with SEM.

(E–G) Plots showing average responses of synaptophysin-pHluorin to 10 Hz, 75 stimuli in *Synj1*$^{+/+}$ neurons (black), *Synj1*$^{-/-}$ neurons (red), *Synj1*$^{-/-}$, Synj1 (145-kDa isoform) neurons (E, gray), *Synj1*$^{-/-}$, SYNJ1^{C383S} (F, 145-kDa isoform) neurons (light blue), and *Synj1*$^{-/-}$, SYNJ1^{D730A} (145-kDa isoform) neurons (G, blue). The fluorescence signals are normalized to the peak for each field of view.

(H–J) The percentage of peak fluorescence remaining at 3 s after the peak (H), the percent of peak fluorescence remaining at 30 s from the peak (I), and the number of clathrin-coated vesicles at rest in these neurons (J). Note that there is a trend toward faster recovery in Sac1-dead neurons than in 5-phosphatase-dead neurons.

Bar graphs show mean and SEM. For 10 Hz, 75 stimuli experiments, n = fields of view: wild-type = 4, knockout = 5, *Synj1*$^{-/-}$, SYNJ1 (145-kD) = 10, *Synj1*$^{-/-}$, SYNJ1^{D730A} = 5, *Synj1*$^{-/-}$, SYNJ1^{C383S} = 5. For 20 Hz, 10 stimuli experiments, n = fields of view: wild-type = 5, knockout = 4, *Synj1*$^{-/-}$, SYNJ1 (145-kD) = 9, *Synj1*$^{-/-}$, SYNJ1^{D730A} = 3, *Synj1*$^{-/-}$, SYNJ1^{C383S} = 3. 48–156 synapses per field of view. *p < 0.05, **p < 0.01. See Quantification and Statistical Analysis for the detailed n values and numbers.

3J). The slow quenching observed in both phosphatase mutants suggests that these vesicles with clathrin coats are being acidified very slowly or, alternatively, that clathrin completely blocks acidification and the vesicles are being uncoated asynchronously.

Endophilin Mediates Neck Formation during Ultrafast Endocytosis

Because synaptojanin functions closely with endophilin, we tested the role of endophilin in ultrafast endocytosis. Synaptic endophilins are encoded by three genes, *Sh3gl2*, *Sh3gl1*, and *Sh3gl3*, in the mouse, encoding endophilin 1, 2, and 3, respectively; the triple mutant is referred to hereafter as *EndoA* triple knockout [TKO]) to avoid confusion caused by this nomenclature (Kjaerulff et al., 2011; for complete genotypes, see STAR Methods). As shown previously (Milosevic et al., 2011), double and triple mutants have a defect in synaptic transmission (Figure S3A), but a sufficient number of synaptic vesicles fuse to trigger compensatory endocytosis. To determine which isoforms function in ultrafast endocytosis, we analyzed single, double, and triple mutants 100 ms and 3 s after stimulation. We found that single mutants are normal but double and triple mutants are defective for ultrafast endocytosis. After flash-and-freeze (a single stimulus, 37°C, 4 mM Ca^{2+}), *EndoA1* knockout (KO)

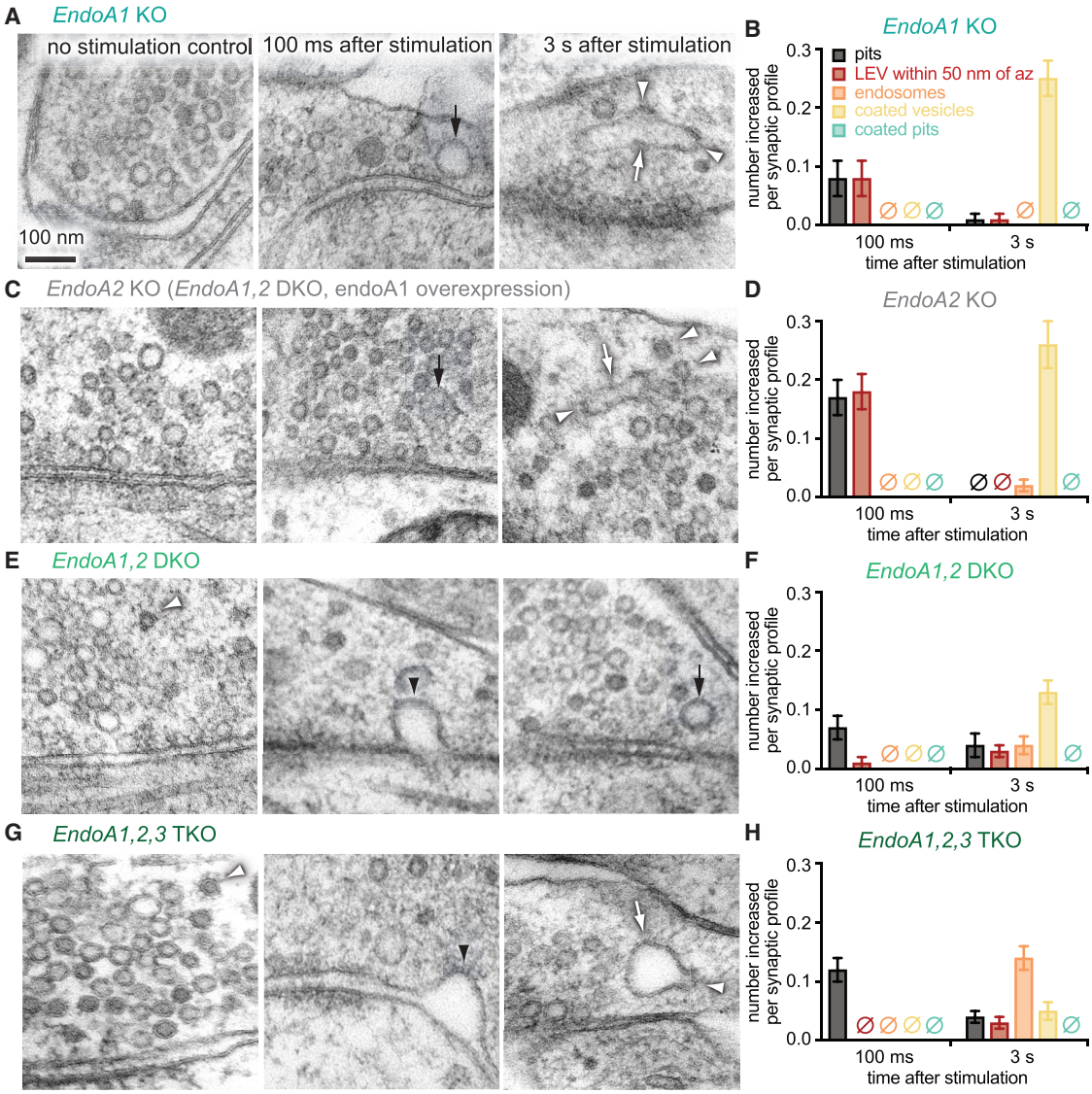

Figure 4. Either EndoA1 or EndoA2 Can Provide Endophilin Function for Endocytosis

(A, C, E, and G) Example micrographs showing endocytic structures at the indicated time points in (A) *EndoA1* knockout neurons, (C) *EndoA2* knockout neurons (*EndoA1,2* DKO with *EndoA1* rescue), (E) *EndoA1,2* DKO neurons, and (G) *EndoA1,2,3* triple knockout neurons. Black arrowheads, endocytic invaginations; black arrows, large endocytic vesicles; white arrows, endosomes; white arrowheads, clathrin-coated vesicles. Note that the endocytic defect can be rescued when either ENDO A1 or ENDO A2 is present.

(B, D, F, and H). Plots showing increases in the number of each endocytic structure per synaptic profile after a single stimulus in *EndoA1* knockout neurons (B), *EndoA2* knockout neurons (D), *EndoA* DKO neurons (F), and *EndoA* triple knockout neurons (H). "LEV" represents large endocytic vesicles located within 50 nm of both the plasma membrane and the edge of the active zone. The mean and SEM are shown in each graph. n = 2 cultures.

See Quantification and Statistical Analysis for the n values and detailed numbers for each time point. See Figure S4 for additional images.

and *EndoA2* knockout single mutants exhibited normal ultrafast endocytosis (Figures 4 and S4). Like the wild-type at 100 ms, half of the endocytic structures are already internalized in *EndoA1* knockout and *EndoA2* knockout (Figures 4A–4D, S4A, and S4B). By contrast, in the *EndoA1,2* double knockout (DKO) or in the *EndoA* triple knockout, all endocytic structures are still connected with the plasma membrane 100 ms after stimulation (Figures 4E–4H, S4C, and S4D). These data suggest that ENDOA1 and ENDOA2 can each mediate endophilin function during ultrafast endocytosis and that ENDOA3 does not contribute significantly.

To fully characterize the role of endophilin in ultrafast endocytosis, we performed a complete time course of flash-and-freeze experiments on the *EndoA1,2* DKO and *EndoA* triple knockout. A single stimulus of 10 ms was applied, and cells were frozen at the indicated time points (Figures 5 and S5; 37°C, 4 mM Ca^{2+}). In both DKO and triple knockout mutants, ultrafast endocytic pits were observed at 30 ms and 100 ms as in the wild-type

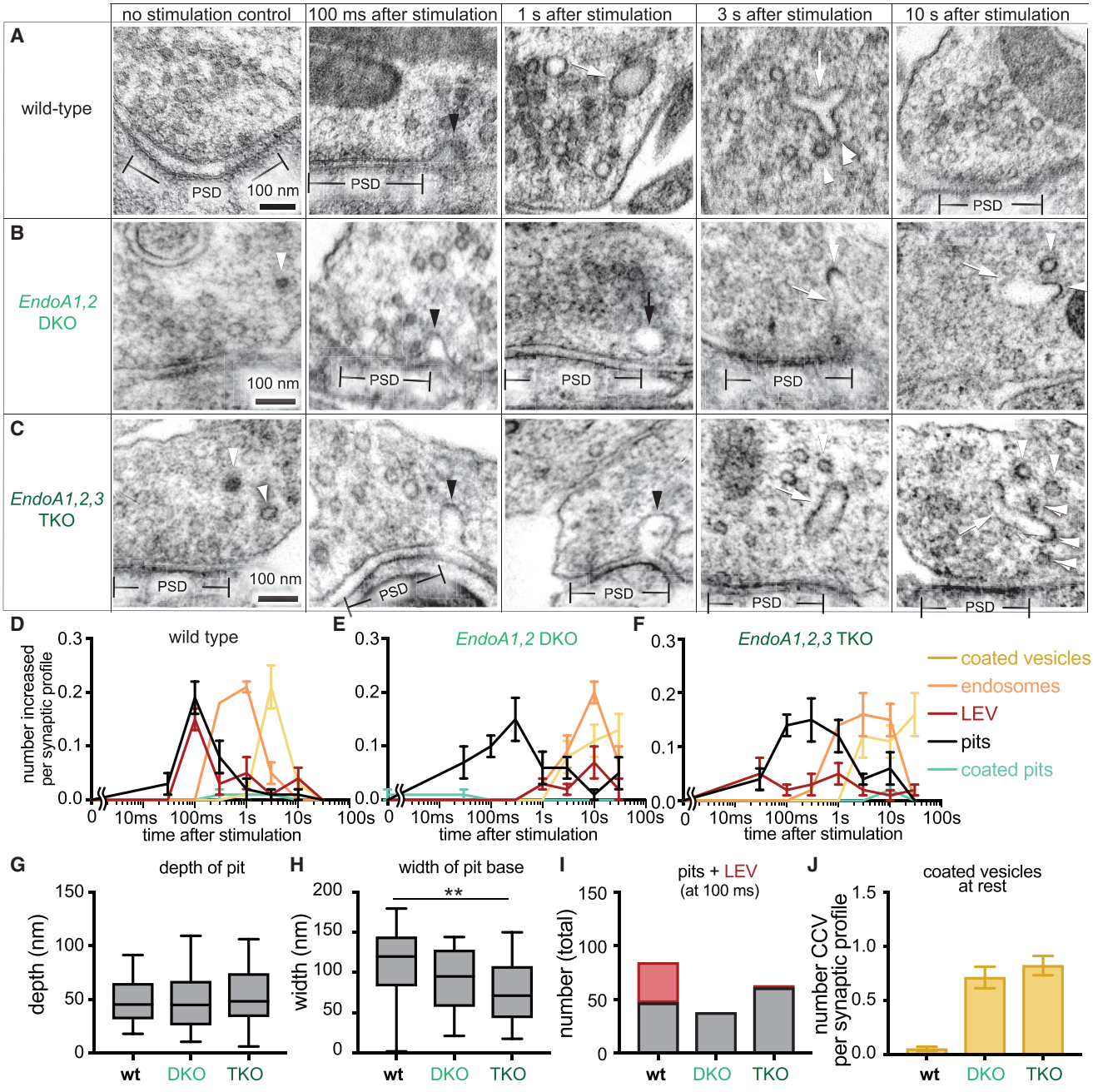

Figure 5. Endophilin Is Necessary for Efficient Neck Formation of Endocytic Vesicles during Ultrafast Endocytosis

(A–C) Example electron micrographs representing endocytic intermediates at the indicated time points in wild-type neurons (A), *EndoA* DKO neurons (B), and *EndoA* triple knockout neurons (C). Black arrowheads, endocytic invaginations; black arrows, large endocytic vesicles; white arrows, endosomes; white arrowheads, clathrin-coated vesicles. "LEV" represents large endocytic vesicles located within 50 nm of both the plasma membrane and the edge of the active zone. Note that endocytic invaginations and clathrin-coated vesicles persist longer in the *EndoA* DKO and triple knockout neurons.

(D–F) Plots showing increases in the number of each endocytic structure per synaptic profile after a single stimulus in wild-type neurons (D), *EndoA* DKO neurons (E), and *EndoA* triple knockout neurons (F). The mean and SEM are shown in each graph.

(G and H) Box and whisker plots showing the median width (G) and height (H) of endocytic invaginations at 100 ms. Note that, in the wild-type, some necks have closed (0 nm).

(I) Total number of endocytic pits and large endocytic vesicles found at the 100-ms time point in the respective genotypes.

(J) Number of clathrin-coated vesicles in the resting terminals (mean ± SEM). n = 2 cultures.

See Quantification and Statistical Analysis for the n values and detailed numbers for each time point. **p < 0.01. See Figure S5 for additional images.

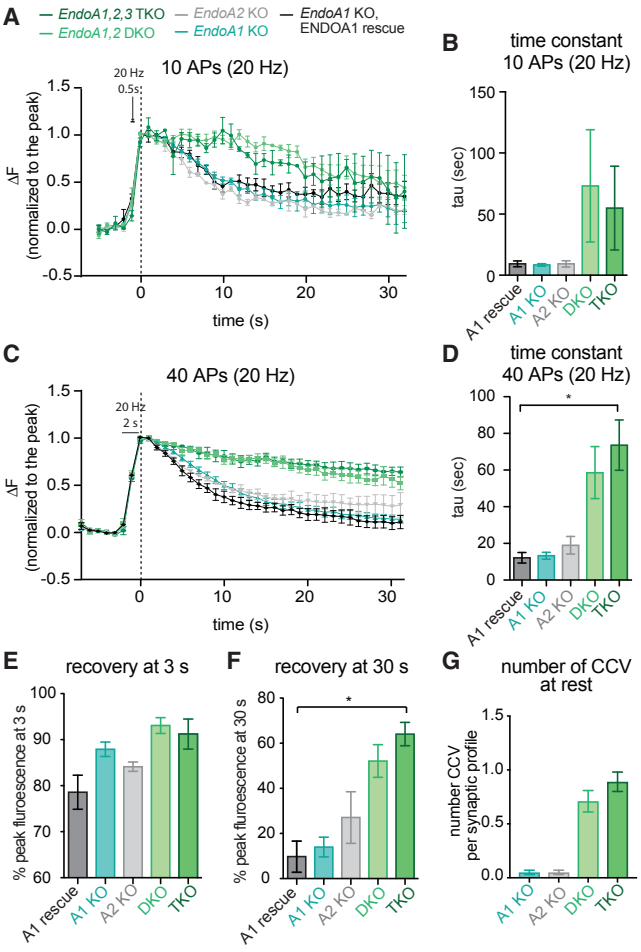

Figure 6. Expression of Endophilin A1 or Endophilin A2 Is Required for Vesicle Acidification at 35°C

(A and B) Plots showing averaged responses of synaptophysin-pHluorin to a 20-Hz train of 10 stimuli (A) or 40 stimuli (B) in *EndoA1* knockout rescue neurons (EndoA1 knockout, ENDO A1 rescue, black), *EndoA2* knockout neurons (*EndoA1, 2* DKO with ENDO A1 rescue, gray), *EndoA1* knockout neurons (teal), *EndoA1,2* DKO neurons (light green), and *EndoA1,2,3* triple knockout neurons (dark green). The fluorescence signals are normalized to the peak fluorescence for each field of view.

(B and D) The time constant for fluorescence recovery following 20 Hz, 10 stimuli (B) and 20 Hz, 40 stimuli (D). The time constant for recovery was obtained by fitting each pHluorin decay with a single exponential decay. Time constants are shown as mean with SEM.

(C and D) Plots showing the percentage of peak fluorescence remaining at 3 s (C) and 30 s (D) after peak in the indicated genotypes.

(E) Number of clathrin-coated vesicles per synaptic profile at rest.

All graphs indicate SE. For 20 Hz, 40 stimuli experiments, n = fields of view: *Endo A1* knockout rescue, 4; *EndoA1* knockout, 4; *EndoA2* knockout, 2; *Endo A* DKO, 4; *EndoA* triple knockout, 4. For 20 Hz, 10 stimuli experiments, n = fields of view: *Endo A1* knockout rescue, 3; *EndoA1* knockout, 4; *EndoA2* knockout, 2; *Endo A* DKO, 3; *EndoA* triple knockout, 2. Each field of view is an average of 59–151 selected puncta. Fields of view are from 2 cultures (*EndoA* triple knockout, *EndoA* DKO, *EndoA1* knockout) or 1 culture (*EndoA2* knockout, *EndoA1* knockout rescue). *p < 0.05. See Quantification and Statistical Analysis for the detailed n values and numbers.

(Figures 5A, 5D, 5F, 5I, and S5A). However, pits were still present at 1 s in the mutants (Figures 5B, 5C, 5E, 5F, S5B, and S5C), whereas they were mostly resolved in the wild-type. Similar to the wild-type, the depths of endocytic pits in the mutants were ~50 nm (100 ms: wild-type 47.8 ± 2.9 nm; DKO 48 ± 3.6 nm; triple knockout 54 ± 3.0 nm; Figure 5G). Typically, the widths of pits were narrower in the DKO and triple knockout mutants than in the wild-type (Figure 5H; mean wild-type 103.5 ± 8.6 nm, n = 47 pits; *EndoA* DKO 89.2 ± 6.1 nm, n = 38 pits; *EndoA* triple knockout 74.6 ± 4.6 nm, n = 61 pits). However, in a substantial fraction of wild-type synapses, the width of the neck was narrower than 5 nm (10 of 47 pits; Figures S3B and S3C), whereas, in endophilin mutants, none of the necks were smaller than 20 nm, suggesting that endophilin is needed to narrow the neck of the pit as the vesicle forms (Figures 5B and 5C; 100 ms and 1 s). Ultrafast endocytosis in endophilin DKO and triple knockout mutants is slowed, but pits decline in number after 3 s, although some pits linger until 30 s (Figures 5D–5F). The decline of pits is not due to failure of endocytosis because the products of endocytosis, large endocytic vesicles and endosomes, are observed at later time points (Figures 5B, 5C, S5B, and S5C). Clathrin-coated vesicles are formed from synaptic endosomes, but, like synaptojanin mutants, clathrin-coats persist on vesicles (Figures 5B–5F and 5J), suggesting that endophilin is required for clathrin uncoating (Milosevic et al., 2011).

Coated Vesicles Are Not Acidified

To determine the role of endophilin in acidification of synaptic vesicles, we analyzed quenching of pHluorin-tagged synaptophysin in *EndoA* knockout neurons. Cultured hippocampal neurons from endophilin knockout mice were stimulated at 20 Hz for 0.5 s (Figures 6A and 6B) or 2 s (Figures 6C and 6D) at 35°C. In *EndoA* DKO and triple knockout neurons, quenching of pHluorin was substantially delayed compared with the EndoA1 knockout rescue (Figure 6B; 10 action potentials, DKO τ = 73 s, triple knockout τ = 55 s, EndoA1 rescue τ = 9 s; Figure 6D; DKO τ = 59 s, triple knockout τ = 74 s, EndoA1 rescue τ = 12 s, $p < 0.05$). Endophilin A1 and A2 single knockout neurons have kinetics much more similar to the Endo A1 knockout rescue phenotype (Figure 6B; 20 action potentials; *EndoA1* knockout τ = 8 s, *EndoA2* knockout τ = 9 s Figures 6D; 40 action potentials; *EndoA1* knockout τ = 13 s, *EndoA2* knockout τ = 19 s). These data suggest that ENDOA1 and ENDOA2 can function independently to sustain normal synaptic vesicle endocytosis. This is in agreement with our flash-and-freeze data as well as previous data (Milosevic et al., 2011), in which the defect in compensatory endocytosis in *EndoA* triple knockout was rescued by transfection of ENDOA1 alone.

These data also demonstrate a correlation between acidification and uncoating of vesicles. In the pHluorin experiments in the *EndoA1* knockout rescue (40 action potential stimulus), 65% of the synaptophysin-pHluorin signal was quenched within 10 s and 90% quenched at 30 s (Figure 6D). These data suggest that uncoated vesicles are acidified. In pHluorin experiments in endophilin DKO and triple knockout mutants, only 22% of synaptophysin-pHluorin was quenched by 10 s after the stimulus and only 48% and 36%, respectively, after 30 s (Figure 6D). In flash-and-freeze experiments, coated vesicles were abundant 10–30 s

after the stimulus in these mutants. One interpretation of the pHluorin experiments is that endophilin and synaptojanin are directly required for acidification of vesicles. An alternative and simpler interpretation is that only uncoated vesicles can be fully acidified to the synaptic vesicle pH (5.5). These data are consistent with recent studies demonstrating that the clathrin lattice can block the activity of the vacuolar ATPase (Farsi et al., 2018).

DISCUSSION

After single action potentials at physiological temperature, synaptic vesicle membranes are not recycled by clathrin but, rather, by ultrafast endocytosis, which is clathrin-independent (Delvendahl et al., 2016; Soykan et al., 2017; Watanabe et al., 2013a, 2013b, 2014). We find that synaptojanin and endophilin are required during ultrafast endocytosis to narrow the neck of an invagination to promote scission of the vesicle from the membrane. The speed with which these proteins can act—as rapidly as 30 ms—is surprising (Watanabe et al., 2013a). The speed of diffusion would normally impose severe limits on the assembly of protein complexes; however, assembly could be greatly accelerated by being in the enclosed space of a synaptic varicosity and localized to membranes (Yogurtcu and Johnson, 2018).

Although ultrafast endocytosis is clathrin-independent, these results also have implications for clathrin-mediated endocytosis. Previous morphological studies of clathrin-mediated endocytosis in synaptojanin and endophilin mutants did not reveal defects in endocytosis (Cremona et al., 1999; Hayashi et al., 2008; Milosevic et al., 2011). The problem arises because traditional fixation cannot capture transient events. Clathrin-mediated endocytosis is merely slowed in these mutants, not blocked (Mani et al., 2007). By using flash-and-freeze electron microscopy, we can capture transient states. Normally, endocytic pits are resolved by 300 ms, but these persist for 30 s in synaptojanin and endophilin mutants. It is likely that the mechanisms for synaptojanin and endophilin function are conserved in clathrin-mediated endocytosis.

Synaptojanin 5-Phosphatase Cinches the Neck of Endocytic Pits

Synaptojanin possesses two phosphatidylinositol phosphatase domains: the 5-phosphatase, which removes the phosphate from the 5 position of the inositol ring from $PI(4,5)P_2$ or $PI(3,4,5)P_3$, and the Sac1 domain, which removes phosphates from the 3 or 4 positions of the inositol ring from PI3P, PI4P, or $PI(3,5)P_2$ (Guo et al., 1999; Nemoto et al., 2001). In the synaptojanin-null mutant, ultrafast endocytosis is stalled as shallow pits with a wide base. The 5-phosphatase-specific mutant exhibits an identical phenotype as the null, but no endocytosis defect is observed in the absence of the 4-phosphatase. This stepwise conversion of $PI(4,5)P_2$ to PI4P, rather than to phosphatidylinositol (PI), is consistent with the progression of phosphoinositides observed in clathrin-mediated endocytosis (He et al., 2017). The stalled endocytic pits in synaptojanin mutants are eventually resolved by 30 s, demonstrating that loss of the 5-phosphatase creates a kinetic, rather than an absolute, block of endocytosis. However, we cannot exclude the possibility that another 5-phosphatase, such as OCRL, eventually functions to resolve the endocytic pit.

These data are consistent with studies of ultrafast endocytosis at synapses in the nematode. Ultrafast endocytosis occurs even at room temperature in *C. elegans* (Watanabe et al., 2013a) and does not require clathrin (Sato et al., 2009). In synaptojanin mutants, uncoated pits with broad necks are observed (Harris et al., 2000), and the 5-phosphatase alone is sufficient to rescue evoked responses (Dong et al., 2015). These studies indicate that the catalytic activity of Sac1 is dispensable for ultrafast endocytosis.

There is a similar requirement for 5-phosphatase activity during clathrin-mediated endocytosis in cultured cortical neurons at 22°C (Mani et al., 2007). Endocytosis was assayed by acidification of pHluorin-tagged synaptobrevin *during* or *after* a stimulation train (30 s of 10 Hz). Acidification *during* stimulation represents a significant fraction of the total protein recovered, more than 50%, and is strongly dependent on the 5-phosphatase but not the 4-phosphatase activity of synaptojanin. Endocytosis and acidification occurring *after* stimulation at 22°C depended on both the 5-phosphatase and the 4-phosphatase activity of synaptojanin. These data suggest that clathrin-mediated endocytosis requires the 5-phosphatase during, but not after, stimulation. Alternatively, the 5-phosphatase-specific defect could imply that ultrafast endocytosis occurs during stimulation even at 22°C.

Although we imagine that $PI(4,5)P_2$ hydrolysis is specifically needed for endocytosis, it is also possible that the defect in ultrafast endocytosis observed in synaptojanin mutants is due to an indirect effect of $PI(4,5)P_2$ accumulation. For example, the NALCN sodium channels appear to be constitutively active in synaptojanin mutants in *C. elegans* (Jospin et al., 2007). Alternatively, $PI(4,5)P_2$ accumulation could increase membrane tension via the cortical actin network (Di Paolo and De Camilli, 2006). In either case, increased membrane tension because of increased osmolarity or by cortical actin may hinder membrane invagination. However, the fact that loss of endophilin, a membrane-bending protein, leads to the same phenotype suggests that synaptojanin actively participates in membrane reshaping. Genetic studies in *C. elegans* and in *Drosophila* suggest that these two proteins function interdependently on the same process (Schuske et al., 2003; Verstreken et al., 2003).

Endophilin and Neck Constriction

Like the 5-phosphatase of synaptojanin, endophilin is required to narrow the neck during ultrafast endocytosis. BAR domains can bind and tubulate membranes *in vitro* (Farsad et al., 2001; Frost et al., 2009; Peter et al., 2004); in addition, endophilin possesses amphipathic helices that insert into the membrane to actively generate curvature (Capraro et al., 2013; Gallop et al., 2006; Poudel et al., 2016). We observed that endophilin is required *in vivo* to cinch the base of endocytic pits from their initial diameter of 100 nm to cleavage; in mutants, the neck is never narrower than 20 nm. Nevertheless, these stalled pits are eventually resolved by 30 s.

There is a similar requirement for endophilin during clathrin-dependent endocytosis at 22°C (Milosevic et al., 2011); specifically, endophilin accelerates endocytosis but is not essential for synaptic vesicle regeneration. Recovery of the membrane, measured by pHluorin quenching, was slowed from a time

constant of 29 s in the wild-type to 71 s in the endophilin triple knockouts after a 10-Hz stimulation. Stalled coated pits were not observed in the endophilin mutants at room temperature; again, because the defect is kinetic rather than absolute, pits would not be expected to appear in electron micrographs.

Endophilin also drives another form of clathrin-independent endocytosis called fast endophilin-mediated endocytosis (FEME). FEME mediates the recovery of synaptic vesicles at ribbon synapses (Llobet et al., 2011) and of G-protein and tyrosine kinase receptors in fibroblasts and epidermal cells (Boucrot et al., 2015; Renard et al., 2015). In this endocytic pathway, endophilin is thought to recruit cargo by direct interaction via its SH3 domain and to act as a coat protein to generate curvature (Boucrot et al., 2015). In our experiments, we did not observe a defect in the invagination of membrane, so it is unlikely that endophilin drives invagination during ultrafast endocytosis; nevertheless, FEME and ultrafast endocytosis may be related, given the rapid speed observed for these mechanisms.

Model for Endophilin and Synaptojanin in Vesicle Cleavage

The similarity in mutant phenotypes suggests that synaptojanin and endophilin act together during ultrafast endocytosis. Moreover, double mutants lacking both synaptojanin and endophilin are identical to single mutants in worms and flies (Schuske et al., 2003; Verstreken et al., 2002, 2003); knocking out one protein is equivalent to knocking out both. Endophilin is required to recruit synaptojanin to endocytic sites in worms, flies, and mice (Milosevic et al., 2011; Schuske et al., 2003; Verstreken et al., 2003). How endophilin recruits synaptojanin is somewhat controversial. In mice, the SH3 domain of endophilin binds the proline-rich domain of synaptojanin and recruits it to the membrane (Frost et al., 2009; Milosevic et al., 2011; Peter et al., 2004), whereas, in *C. elegans*, the BAR domain of endophilin appears to act via the Sac1 domain of synaptojanin (Dong et al., 2015).

The ultimate arbiter of vesicle cleavage is undoubtedly dynamin. Temperature-sensitive mutants or pharmacological inhibition of dynamin leads to stalled pits with narrow necks during ultrafast endocytosis (Watanabe et al., 2013a, 2013b). It is therefore likely that endophilin and synaptojanin work together to generate a tubule, less than 20 nm in diameter, that is then a substrate for dynamin to cleave the vesicle from the membrane. Apparently, in the absence of synaptojanin or endophilin, dynamin can eventually cleave the vesicle from the membrane on its own, albeit inefficiently. This conclusion is consistent with experiments demonstrating that endophilin operates in an additive manner with dynamin to cleave tubules during clathrin-independent Shiga toxin entry (Renard et al., 2015).

How might synaptojanin and endophilin work together to promote vesicle formation during ultrafast endocytosis? A model for endocytosis in yeast suggests that endophilin and synaptojanin create a positive feedback loop that leads to cleavage of the vesicle (Liu et al., 2009). In this model, the BAR domain of endophilin preferentially binds high-curvature membranes containing $PI(4,5)P_2$ (Chang-Ileto et al., 2011; Yoon et al., 2012) and creates a protective collar that blocks its degradation. Synaptojanin is recruited to the edge of the collar and begins converting $PI(4,5)P_2$ to PI4P. In the proposed model, the neck becomes unstable because of changes in surface tension that can occur in $PI(4,5)P_2$-enriched membranes, created through hydrogen bonding with water (Levental et al., 2008). However, these hydrogen bonds between $PI(4,5)P_2$ are likely already disrupted under the ionic conditions of the cell, and this model is therefore unlikely to fully account for neck formation. PI4P occupies less than half of the surface area $PI(4,5)P_2$ does under normal ionic conditions (Levental et al., 2008). Thus, it is possible that hydrolysis of $PI(4,5)P_2$ to PI4P causes the neck to collapse at the interface. In addition, endophilin necks can create a diffusion barrier that slows diffusion of lipids through the collar *in vitro* (Simunovic et al., 2017), and the pulling force generated by actin could possibly contribute to collapse of the neck (Renard et al., 2015; Simunovic et al., 2017). As the neck contracts, endophilin is recruited to the increased curvature of the tubule (Renard et al., 2015), and the phosphatase activity of synaptojanin is stimulated by increasing curvature (Chang-Ileto et al., 2011), thereby closing the positive feedback loop, restricting the diameter of the neck and facilitating dynamin-mediated fission (Chang-Ileto et al., 2011). This model would require endophilin to be flexible enough to accommodate tubes of different diameters, which is consistent with variable-diameter tubes observed in cryoelectron microscopy (cryo-EM) studies of membrane-bound endophilin (Mim et al., 2012).

The Role of Synaptojanin and Endophilin in Removing Clathrin Coats

The original biochemical characterization identified endophilin as a binding partner of synaptojanin and dynamin (Micheva et al., 1997; Ringstad et al., 1997), suggesting that these proteins are involved in the process of membrane cleavage during endocytosis. Surprisingly, ultrastructural characterizations of synaptojanin and endophilin mutants in worms, flies, and mice indicated that these proteins instead play a role in removing clathrin coats from fully formed vesicles (Cremona et al., 1999; Harris et al., 2000; Milosevic et al., 2011; Schuske et al., 2003; Verstreken et al., 2003); instead of observing stalled coated pits at the plasma membrane, coated vesicles were abundant in the cytoplasm. Our observations resolve these conflicting results, but only in part. Rapid freezing after stimulation demonstrated defects in membrane scission during endocytosis, but this does not easily explain how these proteins function in removing clathrin coats from vesicles.

The coated vesicles we observe at synapses do not arise via endocytosis at the plasma membrane but, rather, via budding from synaptic endosomes that form after ultrafast endocytosis (Watanabe et al., 2014). Nevertheless, the mechanism of clathrin-mediated budding of synaptic vesicles from an endosome at 37°C is analogous (and possibly identical) to clathrin-mediated formation of synaptic vesicles from the plasma membrane at 22°C. At 37°C, coated vesicles accumulate after stimulation in synaptojanin and endophilin mutants and do not decline by 30 s, the last time point in our experiments.

Both the 4-phosphatase and the 5-phosphatase activities of synaptojanin are required for uncoating. A Parkinson's disease mutation that disrupts the 4-phosphatase of the Sac1 domain exhibited accumulation of coated vesicles at synapses (Cao

et al., 2017). We found that the 4-phosphatase is specifically required for uncoating vesicles but is not required for endocytosis. The 5-phosphatase is also required for uncoating vesicles, in addition to its role in endocytosis. In the simplest model, the 4-phosphatase and the 5-phosphatase convert $PI(4,5)P_2$ to PI; depletion of $PI(4,5)P_2$ causes release of the clathrin adaptor complex AP2 (Gaidarov et al., 1999). In a second model, the 5-phosphatase specifically catalyzes disassembly of the clathrin lattice; the generation of PI4P recruits auxilin, and, in turn, auxilin catalyzes the dissociation of clathrin triskelions from the coated vesicle (Guan et al., 2010). However, no defect in recruitment of auxilin was detected in the endophilin mutant (Milosevic et al., 2011). In a third model, the 4-phosphatase acts directly, and the 5-phosphatase acts indirectly. The Sac1 4-phosphatase cannot act on $PI(4,5)P_2$ but only PI4P (Guo et al., 1999; Nemoto et al., 2001). Conceivably, the 5-phosphatase could act first during endocytosis to generate PI4P, and the 4-phosphatase could act during uncoating to generate PI and cause the release of the AP2 complex. It is likely that endophilin plays an indirect role; it recruits synaptojanin to the vesicle during scission from the endosome.

It is important to note that defects in clathrin uncoating can confound pHluorin assays of endocytosis. The clathrin lattice inhibits the vacuolar-type H+-ATPase (V-ATPase) (Farsi et al., 2018). Defects in uncoating as well as defects in endocytosis will delay acidification. Finally, like in endocytosis, the loss of synaptojanin and endophilin does not cause an absolute block in uncoating. Vesicle reacidification is slowed but not blocked in these mutants, suggesting that clathrin is being removed during the 30-s time course of our experiments. Although we did not observe full recovery of uncoated vesicles in our ultrastructural assays, functional vesicles must eventually be regenerated because rested synapses can sustain high levels of exocytosis. Again, synaptojanin and endophilin accelerate the processes of endocytosis and uncoating but are not essential for these processes.

STAR★METHODS

Detailed methods are provided in the online version of this paper and include the following:

- KEY RESOURCES TABLE
- CONTACT FOR REAGENT AND RESOURCE SHARING
- EXPERIMENTAL MODEL AND SUBJECT DETAILS
- METHOD DETAILS
  - Culture
  - Expression constructs
  - Lentivirus production and infection
  - Western blots and immunocytochemical staining
  - Flash-and-freeze experiments
  - Freeze-substitution and plastic embedding
  - Ultramicrotomy and electron microscopy
  - pHluorin imaging
  - Electrophysiology
- QUANTIFICATION AND STATISTICAL ANALYSIS
  - Electron microscopy
  - pHluorin imaging
- DATA AND SOFTWARE AVAILABILITY

SUPPLEMENTAL INFORMATION

Supplemental Information includes five figures and one table and can be found with this article online at https://doi.org/10.1016/j.neuron.2018.06.005.

ACKNOWLEDGMENTS

We would like to thank Marta Orlando, Shu-Wen Chang, Marcial Camacho-Pérez, Tanja Rosenmund, Katja Pötschke, Bettina Brokowski, Rike Dannenberg, Sabine Lenz, and the Charité Viral Core Facility for technical assistance; Louis Kerr for providing access to electron microscopy at the Marine Biological Laboratory; and Pietro de Camilli and Timothy A. Ryan for reagents and lively discussions. We thank the Tzagournis Medical Research Endowment Fund for the Ohio State University College of Medicine Medical Student Research Scholarship (to L.E.M.). We thank EMBO (ASTF 443-2012) and the Grass Foundation for providing a fellowship (to S.W.). The research was funded by the Johns Hopkins University start-up funds (to S.W.), the Johns Hopkins University discovery award (to S.W.), the University of Chicago – MBL Lillie award (to S.W., E.M.J., and C.R.), the National Science Foundation (1727271 to S.W.), the NIH (NS034307 to E.M.J.), a European Research Council grant (249939 SYNVGLUT to C.R.), and German Research Council grants (Neurocure EXC 257 to E.M.J. and C.R., SFB 665 and SFB 958 to C.R., and SFB889 and Emmy Noether to I.M.). S.W. is an Alfred P. Sloan fellow. E.M.J. is an Investigator of the Howard Hughes Medical Institute and an Alexander von Humboldt Scholar.

AUTHOR CONTRIBUTIONS

S.W., L.E.M., C.R., and E.M.J. conceived and designed experiments and wrote the manuscript. S.W. and B.S.-K. performed the freezing experiments. S.W., S.R., D.L., and J.E. performed electron microscopy imaging and analysis. L.E.M. and P.F. prepared the cultures, and L.E.M. performed pHluorin imaging and analysis. T.T. generated rescue constructs and the lentivirus. I.M. from the de Camilli lab generated knockout mice. S.W., C.R., and E.M.J. provided funding.

DECLARATION OF INTERESTS

The authors declare no competing interests.

Received: March 22, 2018
Revised: May 12, 2018
Accepted: June 4, 2018
Published: June 27, 2018

REFERENCES

Balaji, J., and Ryan, T.A. (2007). Single-vesicle imaging reveals that synaptic vesicle exocytosis and endocytosis are coupled by a single stochastic mode. Proc. Natl. Acad. Sci. USA *104*, 20576–20581.

Balaji, J., Armbruster, M., and Ryan, T.A. (2008). Calcium control of endocytic capacity at a CNS synapse. J. Neurosci. *28*, 6742–6749.

Berndt, A., Schoenenberger, P., Mattis, J., Tye, K.M., Deisseroth, K., Hegemann, P., and Oertner, T.G. (2011). High-efficiency channelrhodopsins for fast neuronal stimulation at low light levels. Proc. Natl. Acad. Sci. USA *108*, 7595–7600.

Boucrot, E., Ferreira, A.P.A., Almeida-Souza, L., Debard, S., Vallis, Y., Howard, G., Bertot, L., Sauvonnet, N., and McMahon, H.T. (2015). Endophilin marks and controls a clathrin-independent endocytic pathway. Nature *517*, 460–465.

Cao, M., Wu, Y., Ashrafi, G., McCartney, A.J., Wheeler, H., Bushong, E.A., Boassa, D., Ellisman, M.H., Ryan, T.A., and De Camilli, P. (2017). Parkinson sac domain mutation in Synaptojanin 1 impairs clathrin uncoating at synapses and triggers dystrophic changes in dopaminergic axons. Neuron *93*, 882–896.e5.

Capraro, B.R., Shi, Z., Wu, T., Chen, Z., Dunn, J.M., Rhoades, E., and Baumgart, T. (2013). Kinetics of endophilin N-BAR domain dimerization and membrane interactions. J. Biol. Chem. *288*, 12533–12543.

Chang-Ileto, B., Frere, S.G., Chan, R.B., Voronov, S.V., Roux, A., and Di Paolo, G. (2011). Synaptojanin 1-mediated PI(4,5)P2 hydrolysis is modulated by membrane curvature and facilitates membrane fission. Dev. Cell *20*, 206–218.

Cremona, O., Di Paolo, G., Wenk, M.R., Lüthi, A., Kim, W.T., Takei, K., Daniell, L., Nemoto, Y., Shears, S.B., Flavell, R.A., et al. (1999). Essential role of phosphoinositide metabolism in synaptic vesicle recycling. Cell *99*, 179–188.

de Heuvel, E., Bell, A.W., Ramjaun, A.R., Wong, K., Sossin, W.S., and McPherson, P.S. (1997). Identification of the major synaptojanin-binding proteins in brain. J. Biol. Chem. *272*, 8710–8716.

Delvendahl, I., Vyleta, N.P., von Gersdorff, H., and Hallermann, S. (2016). Fast, Temperature-Sensitive and Clathrin-Independent Endocytosis at Central Synapses. Neuron *90*, 492–498.

Di Paolo, G., and De Camilli, P. (2006). Phosphoinositides in cell regulation and membrane dynamics. Nature *443*, 651–657.

Dickman, D.K., Horne, J.A., Meinertzhagen, I.A., and Schwarz, T.L. (2005). A slowed classical pathway rather than kiss-and-run mediates endocytosis at synapses lacking synaptojanin and endophilin. Cell *123*, 521–533.

Dong, Y., Gou, Y., Li, Y., Liu, Y., and Bai, J. (2015). Synaptojanin cooperates in vivo with endophilin through an unexpected mechanism. eLife *4*.

Farsad, K., Ringstad, N., Takei, K., Floyd, S.R., Rose, K., and De Camilli, P. (2001). Generation of high curvature membranes mediated by direct endophilin bilayer interactions. J. Cell Biol. *155*, 193–200.

Farsi, Z., Gowrisankaran, S., Krunic, M., Rammner, B., Woehler, A., Lafer, E.M., Mim, C., Jahn, R., and Milosevic, I. (2018). Clathrin coat controls synaptic vesicle acidification by blocking vacuolar ATPase activity. eLife *7*, e32569.

Frost, A., Unger, V.M., and De Camilli, P. (2009). The BAR domain superfamily: membrane-molding macromolecules. Cell *137*, 191–196.

Gad, H., Ringstad, N., Löw, P., Kjaerulff, O., Gustafsson, J., Wenk, M., Di Paolo, G., Nemoto, Y., Crun, J., Ellisman, M.H., et al. (2000). Fission and uncoating of synaptic clathrin-coated vesicles are perturbed by disruption of interactions with the SH3 domain of endophilin. Neuron *27*, 301–312.

Gaidarov, I., Krupnick, J.G., Falck, J.R., Benovic, J.L., and Keen, J.H. (1999). Arrestin function in G protein-coupled receptor endocytosis requires phosphoinositide binding. EMBO J. *18*, 871–881.

Gallop, J.L., Jao, C.C., Kent, H.M., Butler, P.J.G., Evans, P.R., Langen, R., and McMahon, H.T. (2006). Mechanism of endophilin N-BAR domain-mediated membrane curvature. EMBO J. *25*, 2898–2910.

Granseth, B., Odermatt, B., Royle, S.J., and Lagnado, L. (2006). Clathrin-mediated endocytosis is the dominant mechanism of vesicle retrieval at hippocampal synapses. Neuron *51*, 773–786.

Gu, M., Schuske, K., Watanabe, S., Liu, Q., Baum, P., Garriga, G., and Jorgensen, E.M. (2008). Mu2 adaptin facilitates but is not essential for synaptic vesicle recycling in Caenorhabditis elegans. J. Cell Biol. *183*, 881–892.

Gu, M., Liu, Q., Watanabe, S., Sun, L., Hollopeter, G., Grant, B.D., and Jorgensen, E.M. (2013). AP2 hemicomplexes contribute independently to synaptic vesicle endocytosis. eLife *2*, e00190.

Guan, R., Dai, H., Harrison, S.C., and Kirchhausen, T. (2010). Structure of the PTEN-like region of auxilin, a detector of clathrin-coated vesicle budding. Structure *18*, 1191–1198.

Gunaydin, L.A., Yizhar, O., Berndt, A., Sohal, V.S., Deisseroth, K., and Hegemann, P. (2010). Ultrafast optogenetic control. Nat. Neurosci. *13*, 387–392.

Guo, S., Stolz, L.E., Lemrow, S.M., and York, J.D. (1999). SAC1-like domains of yeast SAC1, INP52, and INP53 and of human synaptojanin encode polyphosphoinositide phosphatases. J. Biol. Chem. *274*, 12990–12995.

Harris, T.W., Hartwieg, E., Horvitz, H.R., and Jorgensen, E.M. (2000). Mutations in synaptojanin disrupt synaptic vesicle recycling. J. Cell Biol. *150*, 589–600.

Hayashi, M., Raimondi, A., O'Toole, E., Paradise, S., Collesi, C., Cremona, O., Ferguson, S.M., and De Camilli, P. (2008). Cell- and stimulus-dependent heterogeneity of synaptic vesicle endocytic recycling mechanisms revealed by studies of dynamin 1-null neurons. Proc. Natl. Acad. Sci. USA *105*, 2175–2180.

He, K., Marsland, R., III, Upadhyayula, S., Song, E., Dang, S., Capraro, B.R., Wang, W., Skillern, W., Gaudin, R., Ma, M., and Kirchhausen, T. (2017). Dynamics of phosphoinositide conversion in clathrin-mediated endocytic traffic. Nature *552*, 410–414.

Herman, M.A., Ackermann, F., Trimbuch, T., and Rosenmund, C. (2014). Vesicular glutamate transporter expression level affects synaptic vesicle release probability at hippocampal synapses in culture. J. Neurosci. *34*, 11781–11791.

Heuser, J.E., and Reese, T.S. (1973). Evidence for recycling of synaptic vesicle membrane during transmitter release at the frog neuromuscular junction. J. Cell Biol. *57*, 315–344.

Jospin, M., Watanabe, S., Joshi, D., Young, S., Hamming, K., Thacker, C., Snutch, T.P., Jorgensen, E.M., and Schuske, K. (2007). UNC-80 and the NCA ion channels contribute to endocytosis defects in synaptojanin mutants. Curr. Biol. *17*, 1595–1600.

Kaksonen, M., Toret, C.P., and Drubin, D.G. (2005). A modular design for the clathrin- and actin-mediated endocytosis machinery. Cell *123*, 305–320.

Kim, J.H., Lee, S.-R., Li, L.-H., Park, H.-J., Park, J.-H., Lee, K.Y., Kim, M.-K., Shin, B.A., and Choi, S.-Y. (2011). High cleavage efficiency of a 2A peptide derived from porcine teschovirus-1 in human cell lines, zebrafish and mice. PLoS ONE *6*, e18556.

Kjaerulff, O., Brodin, L., and Jung, A. (2011). The structure and function of endophilin proteins. Cell Biochem. Biophys. *60*, 137–154.

Kononenko, N.L., Puchkov, D., Classen, G.A., Walter, A.M., Pechstein, A., Sawade, L., Kaempf, N., Trimbuch, T., Lorenz, D., Rosenmund, C., et al. (2014). Clathrin/AP-2 mediate synaptic vesicle reformation from endosome-like vacuoles but are not essential for membrane retrieval at central synapses. Neuron *82*, 981–988.

Levental, I., Cebers, A., and Janmey, P.A. (2008). Combined electrostatics and hydrogen bonding determine intermolecular interactions between polyphosphoinositides. J. Am. Chem. Soc. *130*, 9025–9030.

Liu, J., Sun, Y., Drubin, D.G., and Oster, G.F. (2009). The mechanochemistry of endocytosis. PLoS Biol. *7*, e1000204.

Llobet, A., Gallop, J.L., Burden, J.J.E., Çamdere, G., Chandra, P., Vallis, Y., Hopkins, C.R., Lagnado, L., and McMahon, H.T. (2011). Endophilin drives the fast mode of vesicle retrieval in a ribbon synapse. J. Neurosci. *31*, 8512–8519.

Lois, C., Hong, E.J., Pease, S., Brown, E.J., and Baltimore, D. (2002). Germline transmission and tissue-specific expression of transgenes delivered by lentiviral vectors. Science *295*, 868–872.

Mani, M., Lee, S.Y., Lucast, L., Cremona, O., Di Paolo, G., De Camilli, P., and Ryan, T.A. (2007). The dual phosphatase activity of synaptojanin1 is required for both efficient synaptic vesicle endocytosis and reavailability at nerve terminals. Neuron *56*, 1004–1018.

McPherson, P.S., Garcia, E.P., Slepnev, V.I., David, C., Zhang, X., Grabs, D., Sossin, W.S., Bauerfeind, R., Nemoto, Y., and De Camilli, P. (1996). A presynaptic inositol-5-phosphatase. Nature *379*, 353–357.

Micheva, K.D., Kay, B.K., and McPherson, P.S. (1997). Synaptojanin forms two separate complexes in the nerve terminal. Interactions with endophilin and amphiphysin. J. Biol. Chem. *272*, 27239–27245.

Miesenböck, G., De Angelis, D.A., and Rothman, J.E. (1998). Visualizing secretion and synaptic transmission with pH-sensitive green fluorescent proteins. Nature *394*, 192–195.

Miller, T.M., and Heuser, J.E. (1984). Endocytosis of synaptic vesicle membrane at the frog neuromuscular junction. J. Cell Biol. *98*, 685–698.

Milosevic, I., Giovedi, S., Lou, X., Raimondi, A., Collesi, C., Shen, H., Paradise, S., O'Toole, E., Ferguson, S., Cremona, O., and De Camilli, P. (2011).

Recruitment of endophilin to clathrin-coated pit necks is required for efficient vesicle uncoating after fission. Neuron *72*, 587–601.

Mim, C., Cui, H., Gawronski-Salerno, J.A., Frost, A., Lyman, E., Voth, G.A., and Unger, V.M. (2012). Structural basis of membrane bending by the N-BAR protein endophilin. Cell *149*, 137–145.

Nemoto, Y., Wenk, M.R., Watanabe, M., Daniell, L., Murakami, T., Ringstad, N., Yamada, H., Takei, K., and De Camilli, P. (2001). Identification and characterization of a synaptojanin 2 splice isoform predominantly expressed in nerve terminals. J. Biol. Chem. *276*, 41133–41142.

Peter, B.J., Kent, H.M., Mills, I.G., Vallis, Y., Butler, P.J.G., Evans, P.R., and McMahon, H.T. (2004). BAR domains as sensors of membrane curvature: the amphiphysin BAR structure. Science *303*, 495–499.

Poudel, K.R., Dong, Y., Yu, H., Su, A., Ho, T., Liu, Y., Schulten, K., and Bai, J. (2016). A time course of orchestrated endophilin action in sensing, bending, and stabilizing curved membranes. Mol. Biol. Cell *27*, 2119–2132.

Pyott, S.J., and Rosenmund, C. (2002). The effects of temperature on vesicular supply and release in autaptic cultures of rat and mouse hippocampal neurons. J. Physiol. *539*, 523–535.

Renard, H.-F., Simunovic, M., Lemière, J., Boucrot, E., Garcia-Castillo, M.D., Arumugam, S., Chambon, V., Lamaze, C., Wunder, C., Kenworthy, A.K., et al. (2015). Endophilin-A2 functions in membrane scission in clathrin-independent endocytosis. Nature *517*, 493–496.

Ringstad, N., Nemoto, Y., and De Camilli, P. (1997). The SH3p4/Sh3p8/SH3p13 protein family: binding partners for synaptojanin and dynamin via a Grb2-like Src homology 3 domain. Proc. Natl. Acad. Sci. USA *94*, 8569–8574.

Ringstad, N., Nemoto, Y., and De Camilli, P. (2001). Differential expression of endophilin 1 and 2 dimers at central nervous system synapses. J. Biol. Chem. *276*, 40424–40430.

Sato, K., Ernstrom, G.G., Watanabe, S., Weimer, R.M., Chen, C.H., Sato, M., Siddiqui, A., Jorgensen, E.M., and Grant, B.D. (2009). Differential requirements for clathrin in receptor-mediated endocytosis and maintenance of synaptic vesicle pools. Proc. Natl. Acad. Sci. USA *106*, 1139–1144.

Schuske, K.R., Richmond, J.E., Matthies, D.S., Davis, W.S., Runz, S., Rube, D.A., van der Bliek, A.M., and Jorgensen, E.M. (2003). Endophilin is required for synaptic vesicle endocytosis by localizing synaptojanin. Neuron *40*, 749–762.

Shupliakov, O., Löw, P., Grabs, D., Gad, H., Chen, H., David, C., Takei, K., De Camilli, P., and Brodin, L. (1997). Synaptic vesicle endocytosis impaired by disruption of dynamin-SH3 domain interactions. Science *276*, 259–263.

Simunovic, M., Manneville, J.-B., Renard, H.-F., Evergren, E., Raghunathan, K., Bhatia, D., Kenworthy, A.K., Voth, G.A., Prost, J., McMahon, H.T., et al. (2017). Friction Mediates Scission of Tubular Membranes Scaffolded by BAR Proteins. Cell *170*, 172–184.e11.

Soykan, T., Kaempf, N., Sakaba, T., Vollweiter, D., Goerdeler, F., Puchkov, D., Kononenko, N.L., and Haucke, V. (2017). Synaptic Vesicle Endocytosis Occurs on Multiple Timescales and Is Mediated by Formin-Dependent Actin Assembly. Neuron *93*, 854–866.e4.

Stefan, C.J., Padilla, S.M., Audhya, A., and Emr, S.D. (2005). The phosphoinositide phosphatase Sjl2 is recruited to cortical actin patches in the control of vesicle formation and fission during endocytosis. Mol. Cell. Biol. *25*, 2910–2923.

Stewart, S.A., Dykxhoorn, D.M., Palliser, D., Mizuno, H., Yu, E.Y., An, D.S., Sabatini, D.M., Chen, I.S., Hahn, W.C., Sharp, P.A., et al. (2003). Lentivirus-delivered stable gene silencing by RNAi in primary cells. RNA *9*, 493–501.

Thévenaz, P., Ruttimann, U.E., and Unser, M. (1998). A pyramid approach to subpixel registration based on intensity. IEEE Trans. Image Process. *7*, 27–41.

Vardar, G., Chang, S., Arancillo, M., Wu, Y.-J., Trimbuch, T., and Rosenmund, C. (2016). Distinct Functions of Syntaxin-1 in Neuronal Maintenance, Synaptic Vesicle Docking, and Fusion in Mouse Neurons. J. Neurosci. *36*, 7911–7924.

Verstreken, P., Kjaerulff, O., Lloyd, T.E., Atkinson, R., Zhou, Y., Meinertzhagen, I.A., and Bellen, H.J. (2002). Endophilin mutations block clathrin-mediated endocytosis but not neurotransmitter release. Cell *109*, 101–112.

Verstreken, P., Koh, T.-W., Schulze, K.L., Zhai, R.G., Hiesinger, P.R., Zhou, Y., Mehta, S.Q., Cao, Y., Roos, J., and Bellen, H.J. (2003). Synaptojanin is recruited by endophilin to promote synaptic vesicle uncoating. Neuron *40*, 733–748.

Watanabe, S., Liu, Q., Davis, M.W., Hollopeter, G., Thomas, N., Jorgensen, N.B., and Jorgensen, E.M. (2013a). Ultrafast endocytosis at Caenorhabditis elegans neuromuscular junctions. eLife *2*, e00723.

Watanabe, S., Rost, B.R., Camacho-Pérez, M., Davis, M.W., Söhl-Kielczynski, B., Rosenmund, C., and Jorgensen, E.M. (2013b). Ultrafast endocytosis at mouse hippocampal synapses. Nature *504*, 242–247.

Watanabe, S., Trimbuch, T., Camacho-Pérez, M., Rost, B.R., Brokowski, B., Söhl-Kielczynski, B., Felies, A., Davis, M.W., Rosenmund, C., and Jorgensen, E.M. (2014). Clathrin regenerates synaptic vesicles from endosomes. Nature *515*, 228–233.

Weston, M.C., Nehring, R.B., Wojcik, S.M., and Rosenmund, C. (2011). Interplay between VGLUT isoforms and endophilin A1 regulates neurotransmitter release and short-term plasticity. Neuron *69*, 1147–1159.

Yogurtcu, O.N., and Johnson, M.E. (2018). Cytosolic proteins can exploit membrane localization to trigger functional assembly. PLoS Comput. Biol. *14*, e1006031.

Yoon, Y., Zhang, X., and Cho, W. (2012). Phosphatidylinositol 4,5-bisphosphate (PtdIns(4,5)P2) specifically induces membrane penetration and deformation by Bin/amphiphysin/Rvs (BAR) domains. J. Biol. Chem. *287*, 34078–34090.

Zhu, Y., Xu, J., and Heinemann, S.F. (2009). Two pathways of synaptic vesicle retrieval revealed by single-vesicle imaging. Neuron *61*, 397–411.

STAR★METHODS

KEY RESOURCES TABLE

REAGENT or RESOURCE	SOURCE	IDENTIFIER
Antibodies		
Rabbit polyclonal anti-Synj1	de Camilli lab; McPherson et al., 1996	N/A
Mouse anti-Tubulin III	Sigma	Cat# T8660
Bacterial and Virus Strains		
pLenti_f(syn)_hChR2_E123T-T159C-eYFP	Watanabe et al., 2013b	N/A
pLenti_f(syn)-NLS-GFP-P2A-Synj1	This paper	N/A
pLenti_f(syn)-NLS-GFP-P2A-Synj1-C383S-w	This paper	N/A
pLenti_f(syn)-NLS-GFP-P2A-Synj1-D730A	This paper	N/A
pLenti_f(syn)-NLS-GFP-P2A-w	This paper	N/A
pLenti_f(syn)urw-endophilin1	Weston et al., 2011	N/A
pLenti_f(syn)-iCre-RFP-P2A-w	Vardar et al., 2016	N/A
pLenti_f(syn)-NLS-RFP-P2A-w	Vardar et al., 2016	N/A
pLenti_f(syn)-Syp2pHluorin-w	Herman et al., 2014	N/A
Chemicals, Peptides, and Recombinant Proteins		
Trypsin-EDTA	Invitrogen/GIBCO	Cat# 25300-054
DMEM	Invitrogen/GIBCO	Cat# 31966-021
FBS	Invitrogen/GIBCO	Cat# 26140-079
Penicillin-streptomycin	Roche	Cat# 11074440001
Poly-D-lysin	Sigma-Aldrich	Cat# P2636-500MG
Rat tail collagen	Invitrogen/GIBCO	Cat# A10483-01
Acetic acid	Merck	Cat# 1.00063.1011
Fluoro-deoxyuridine	Sigma-Aldrich	Cat# F0503-100MG
Neurobasal A	Invitrogen/GIBCO	Cat# 10888-022
Glutamax	Invitrogen/GIBCO	Cat# 35050
B27	Invitrogen/GIBCO	Cat# 17504-044
Tris-HCL	Roth	Cat# 90903
Cysteine	Sigma-Aldrich	Cat# C7352-25G
$CaCl_2$	Fluka	Cat# 21114
tetrodotoxin	Tocris	Cat# 1078
Poly-L-lysin	Sigma-Aldrich	Cat# P4707
NaCl	Sigma-Aldrich	Cat# S7653-1KG
polyethylenimine	Polysciences	Cat# 23966-2
cOMPLETE protease inhibitor cocktail tablet	Roche Diagnostics GmbH	Cat# 11836153001
HEPES	Merck	Cat# 1.10110.0250
KCl	Sigma-Aldrich	Cat# P9333
Glucose	Sigma-Aldrich	Cat# 49159-1G
$CaCl_2$	Fluka	Cat# 21114
$MgCl_2$	Fluka	Cat# 63020
NBQX	Tocris	Cat# 1044
Bicuculline	Tocris	Cat# 0130
Cationized ferritin	Sigma-Aldrich	Cat# F7879
Glutaraldehyde in anhydrous acetone	EMS	Cat# 16530
Osmium tetroxide	EMS	Cat# RT19132
Uranyl acetate	EMS	Cat# 22400

(*Continued on next page*)

Continued		
REAGENT or RESOURCE	SOURCE	IDENTIFIER
Acetone	EMS	Cat# RT10016
AP5	Tocris	Cat# 0106
Quikchange II Site-Directed Mutagenesis Kit	Agilent	Cat# 200523
Experimental Models: Organisms/Strains		
Synj1 KO (B6;129-*Synj1*^{tm1Pdc}/J)	Jackson Laboratory	Cat# 013074
EndoA1(B6;129-Sh3gl2^{tm1Pdc}*/J)*$^{-/-}$	Jackson Laboratory	Cat# 21753
EndoA2 (B6;129-Sh3gl1^{tm1Pdc}*/J)*$^{-/-}$	Jackson Laboratory	Cat# 21574
EndoA3$^{loxP/loxP}$*(B6;129-Sh3gl3*$^{tm1.1Itl}$*/J)*	Jackson Laboratory	Cat# 21575
Endophilin A1KO, A2 Het, A3loxP/loxP	Milosevic Laboratory, de Camilli Laboratory, Milosevic et al., 2011; can be created by crossing the three strains above	N/A
Recombinant DNA		
Synaptophysin-pHluorin-2x	Zhu et al., 2009	Addgene Cat# 37004
Synaptojanin-1	This paper	N/A
ChetaTC-YFP	Watanabe et al., 2013b	N/A
f(syn)urw-endophilin1	Weston et al., 2011	N/A
FUGW	Lois et al., 2002	N/A
pCMV-VSV-G	Stewart et al., 2003	N/A
pCMV-dR8.9	Stewart et al., 2003	N/A
Software and Algorithms		
BIO-1D	Fusion FX system	http://www.vilber.de/en/products/analysis-software/bio-1d-advanced/
Morphometry analysis algorithms	S.W. and E.M.J., unpublished data	N/A
MATLAB	MATLAB	https://www.mathworks.com/products/matlab.html
imageJ	NIH	https://imagej.nih.gov/ij/
Prism	GraphPad (Prism 7)	https://www.graphpad.com/
Excel	Microsoft	https://products.office.com/en-us/explore-office-for-home
AxoGraph	AxoGraph	https://axograph.com/
Other		
Sapphire disks, 6-mm	Technotrade	Cat# 616-100
HPM100	Leica microsystem	N/A
AFS2	Leica microsystem	N/A

CONTACT FOR REAGENT AND RESOURCE SHARING

Further information and requests for resources and reagents should be directed to and will be fulfilled by the Lead Contact, Erik M. Jorgensen (jorgensen@biology.utah.edu).

EXPERIMENTAL MODEL AND SUBJECT DETAILS

All of the experiments were performed according to the rules and regulations of animal use by Berlin, Germany authorities and the National Institute of Health. Primary cultures of mouse hippocampal neurons with the following genotypes are used in this study: C57/BL6-N; *Synj1* KO (B6;129-*Synj1*^{tm1Pdc}/J) $^{+/+}$; *Synj1* KO (B6;129-*Synj1*^{tm1Pdc}/J) $^{-/-}$; *EndoA1(B6;129-Sh3gl2*^{tm1Pdc}*/J)*$^{-/-}$, *EndoA2*$^{+/+}$, *EndoA3*$^{loxP/loxP}$*(B6;129-Sh3gl3*$^{tm1.1Itl}$*/J); and EndoA1*$^{-/-}$, *EndoA2 (B6;129-Sh3gl1*^{tm1Pdc}*/J)*$^{-/-}$, *EndoA3*$^{loxP/loxP}$ ± cre recombinase. The *EndoA2* single KO is *EndoA1,2* DKO +EndoA1 rescue; the *EndoA1 EndoA2* double mutant is *EndoA1*$^{-/-}$, *EndoA2*$^{-/-}$, *EndoA3*$^{loxP/\ loxP}$; the *EndoA1 EndoA2 EndoA3* triple mutants is *EndoA1*$^{-/-}$, *EndoA2*$^{-/-}$, *EndoA3*$^{loxP/loxP}$, *+Cre*. The synaptojanin mutation was generated by replacing a genomic fragment containing part of exon 1 and part of intron 1 with a neomycin resistance cassette; western blot analysis of brain tissue demonstrated that no detectable protein was expressed from this allele (Cremona et al., 1999). Hippocampal neurons were isolated from pups of unspecified sex at embryonic day 18 or postnatal day 0.

Adult animals were housed in groups of a single gender whenever possible. In the case of endophilin, experimental animals of the genotype EndoA1$^{-/-}$, Endo A2$^{-/-}$, EndoA3 $^{loxP/loxP}$ and Endo A1$^{-/-}$, Endo A2 $^{+/+}$, and EndoA3 $^{loxP/loxP}$ were generated by crossing EndoA1$^{-/-}$, EndoA2$^{+/-}$, and Endo A3 $^{loxP/loxP}$ animals, which are unaffected as adults (Milosevic et al., 2011). For synaptojanin 1, experimental animals were generated by crossing two Synaptojanin $^{+/-}$ animals, which are also unaffected (Cremona et al., 1999). All protocols were approved by the animal welfare committee of the Charité Berlin, Germany.

METHOD DETAILS

Culture

To prepare primary cultures from mouse hippocampal neurons, the following procedures were carried out. Cortices were dissected from newborn C57/BL6-N mice (both sex, postnatal day 0-1) and treated with 0.05% Trypsin-EDTA for 15 min at 37°C to dissociate astrocytes. The dissociated astrocytes were grown in a 37°C incubator (5% CO_2) to confluency in a T-75 flask with 13 mL DMEM culture media containing 10% FBS and 0.2% penicillin-streptomycin for 1-2 weeks. These astrocytes were then seeded at 3.3x10^4 cells/ml on 22-mm coverslips for pHluorin imaging and 6-mm sapphire disks for flash-and-freeze experiments. Both coverslips and sapphire disks were placed in the wells of 12-well plates and coated with poly-D-lysine (1mg/ml) solution containing rat tail collagen (1 ml) and 17 nM acetic acid (3 ml) prior to seeding. For autaptic cultures used in electrophysiology experiments, this solution was applied on 15-mm glass coverslips placed in the wells of 6-well plates using a custom stamp to create islands of permissive substrate for astrocytes. The astrocytes serve as the feeder layer for hippocampal neurons. The mitosis of astrocytes was then stopped by adding 20 μl fluoro-deoxyuridine (80 μM) following one week of incubation in the 37°C incubator (5% CO_2). The culture media was replaced with Neurobasal A containing 1% glutamax, 2% B27, and 0.2% penicillin-streptomycin. To dissociate hippocampal neurons, cortices and hippocampi were dissected from either P0 mice (synaptojanin) or E18 embryonic mice (endophilin) with the appropriate genotype. Cortices were lysed (10 mM Tris-HCL pH8.0 and 100 mM NaCl in presence of 50 μg proteinase K) to extract DNA for the genotype verification by PCR. To dissociate neurons, hippocampi were incubated at 37°C for 0.5-1 hr in enzyme solution (1.65 mM Cysteine, 1 mM $CaCl_2$, 0.5 mM EDTA in DMEM) containing 20 units of Papain. The dissociated neurons were seeded on the astrocyte feeder layer in the 12-well plates at 6.5x10^4 (electron microscopy), 5x10^4 (pHluorin imaging), or 3x10^3 (electrophysiology) per well and incubated at 37°C for 2 weeks. All the experiments were performed 13-18 days *in vitro* (DIV13-18). To reduce the number of clathrin-coated vesicles in the resting terminal, neurons were routinely incubated with 100 nM tetrodotoxin overnight prior to the experiments and washed 5 min before the sample loading. However, this treatment was not particularly helpful, since there was no significant difference in coated vesicle accumulation when this step was omitted. For biochemistry, 10x10^3 cells/cm^2 were cultured without the feeder layer in 6-well plates.

Expression constructs

Lentiviral expression constructs were used to express transgenes in neurons. All vectors were based on the lentiviral shuttlevector FUGW (Lois et al., 2002). For flash-and-freeze, a variant of channelrhodopsin ChetaTC-YFP (Berndt et al., 2011; Gunaydin et al., 2010) was cloned into this vector; the expression was controlled by the human synapsin 1 promoter (f(syn)-ChetaTC-YFP-w) (Watanabe et al., 2013b). The cDNA of the 145kDa isoform (1309 aa) of Synaptojanin 1 was amplified from the cDNA library of mouse brain and cloned in frame downstream of a synapsin-1 promoter with NLS-GFP-P2A (NGP) sequence. The GFP signals allowed us to evaluate viral infection and intensity of transgene expression from this polycistronic construct (Kim et al., 2011). The mutant versions of synaptojanin (SYNJ1^{C383S} and SYNJ1^{D730A}) were generated from the synaptojanin wild-type cDNA using the Quikchange II Site-Directed Mutagenesis Kit (Agilent). Sequence verified mutant cDNA was subsequently cloned in the lentiviral vector with synapsin-1 promoter and NGP expression cassette (f(syn)-NGP-Synj1-C383S-w, f(syn)-NGP-Synj1-D730A). For the control, GFP was expressed in the nucleus (f(syn)-NLS-GFP-P2A-w). For endophilin-1, mouse EndoA1 cDNA (NCBI genebank U58886.1) was cloned into a lentiviral vector. Additional ubiquitin promoter was added to the expression of RFP to visualize infected neurons (f(syn)urw-endophilin1) (Weston et al., 2011). For the expression of Cre recombinase, the C terminus of a codon-improved Cre (iCre) was fused to RFP. The construct is then cloned into lentiviral vectors with synapsin-1 promoter controlled expression cassette (f(syn)-iCre-RFP-w) (Vardar et al., 2016). For the control, RFP was expressed in nucleus (f(syn)-NLS-RFP-w). For pHluorin imaging a SypHluorin-2x (Zhu et al., 2009) cDNA was cloned into lentiviral vector with the human synapsin-I promoter (f(syn)-Syp2pHluorin-w) (Herman et al., 2014). pcDNA3-SypHluorin 2x (S2x) was a gift from Stephen Heinemann & Yongling Zhu (Addgene plasmid # 37004)).

Lentivirus production and infection

Lentiviruses carrying the expression constructs were produced by the Charité viral core facility (*vcf*.charite.de) using the following procedures. The bottom surface of T-75 flasks were coated with poly-L-lysin (2% in milliQ water). A day before the transfection, HEK293T cells were plated at 6.5x10^5/ml (10 mL in T-75) in Neurobasal A (NBA) media containing 1% glutamax, 2% B27, and 0.2% penicillin-streptomycin. The shuttle vector (FUGW) (Lois et al., 2002) containing expression constructs and helper plasmids (VSV-G and CMV-dR8.9) (Stewart et al., 2003) were mixed at 20, 5, and 7.5 μg, respectively, in 640 μl NaCl solution (150 mM) (Solution I). Another solution (solution II) was prepared as follows: 246.7 μl H_2O, 320 μl NaCl (300 mM), 73.3 μl polyethylenimine (0.6 μg/μl). Solution I and II were mixed, vortexed, and incubated at at room temperature for 10 minutes followed by addition to the T-75 flask containing HEK293T cells. The cells were incubated at 32°C (5% CO_2), and the viruses were harvested 3 days later.

The media containing lentiviruses were centrifuged at 4000 rpm to obtain 20-fold concentration using Amicon tube (Ultra-15, Ultracel-100k). After the centrifugation, the column was topped off with NBA media, resulting in the titer of about 10^7. The infection efficiency is determined by sample infection in wild-type neurons that were not used in the study. For all the experiments, dissociated hippocampal neurons were infected on DIV1-3 with lentiviruses carrying the expression constructs. The infection rate of 100% was achieved in all cases.

Western blots and immunocytochemical staining

For detection of expression levels by western blots, protein lysates were obtained from astrocyte-free mass cultures of hippocampal neurons. Briefly, cells were lysed using 50 mM Tris/HCl (pH 7.9), 150 mM NaCl, 5 mM EDTA, 1% Triton X-100, 1% Nonidet P-40, 1% sodium deoxycholate, and protease inhibitors (cOMPLETE protease inhibitor cocktail tablet, Roche Diagnostics GmbH, Mannheim, Germany). Protein concentration was determined by BCA assay. Proteins were separated by SDS-PAGE and transferred to nitrocellulose membranes. Membranes were then incubated with rabbit anti-synaptojanin-1 (1:300 Gesualdo, gift of de Camilli Lab) and mouse anti-tubulin III (1:2000, Sigma-Aldrich, T8660) antibodies overnight at 4°C. After incubation with corresponding horseradish peroxidase-conjugated goat secondary antibodies (1h at room temperature) and ECL Plus Western Blotting Detection Reagents (GE Healthcare Biosciences), chemiluminescent was imaged using a Vilber Lourmat Fusion FX7 detection system. Ratiometric quantification of signal intensities was measured with the supplied BIO-1D software package of the Fusion FX system.

Flash-and-freeze experiments

Sapphire disks with cultured cells were mounted in the freezing chamber of the high-pressure freezer (HPM100 or EM ICE, Leica), which was set at 37°C. The extracellular solution contained 140 mM NaCl, 2.4 mM KCl, 10 mM HEPES, 10 mM Glucose (pH adjusted to 7.3 with NaOH, 300 mOsm), 4 mM $CaCl_2$, and 1 mM $MgCl_2$. Additionally, NBQX (3 μM) and Bicuculline (30 μM) were added to suppress recurrent network activity following optogenetic stimulation of neurons. To minimize the exposure to room temperature, solutions were kept at 37°C water bath prior to use. The table attached to the high-pressure freezer was heated to ~37°C while mounting specimens on the high-pressure freezer. The transparent polycarbonate sample cartridges were also warmed to 37°C. Immediately after the sapphire disk was mounted on the sample holder, recording solution kept at 37°C was applied to the specimen and the cartridge was inserted into the freezing chamber. The specimens were left in the chamber for 30 s to recover from the exposure to ambient light. Using a custom-built light stimulation controller, we applied 1 light pulse (10 ms) to the specimens (20 mW/mm^2). This stimulation protocol was chosen based on the results from previous experiments showing approximately 90% of cells fire at least one action potential (Watanabe et al., 2013b). The non-stimulation controls for each experiment were always frozen on the same day from the same animal. We set the device so that the samples were frozen at 30, 100, 300, 1000, 3000, 10,000, or 30,000 ms after the initiation of the first stimulus.

For ferritin-loading experiments, cationized ferritin (Sigma-Aldrich) was added in the recording solution at 0.25 mg/ml. The calcium concentration was reduced to 1 mM to suppress spontaneous activity during the loading. The cells were incubated in the solution for 5 min at 37°C. After ferritin incubation, the cells were immersed in the external solution containing 4 mM Ca^{2+}. The change in calcium concentrations from 1 mM to 4 mM increases the rate of miniature EPSCs and thus may contribute to the background ferritin loading before the experiments. In our experiments, about 1% of synaptic profiles contained endosomes and synaptic vesicles that were ferritin-positive without stimulation. The absence of ferritin-positive coated pits on the plasma membrane in the unstimulated controls suggests that ferritin passes through endosomes even during spontaneous activity. Due to space limitation in our automated freeze-substitution unit (AFS2), we omitted earlier time points (100 ms and 300 ms) in ferritin-loading experiments so that all specimens from one group of experiments could be prepared in parallel on the same day. Successful completion of ultrafast endocytosis was evaluated by the presence of ferritin particles in large endocytic vesicles or synaptic endosomes at the 1 s time point.

Freeze-substitution and plastic embedding

Following high-pressure freezing, samples were transferred into a vial containing 1% osmium tetroxide (EMS), 1% glutaraldehyde (EMS), 1% milliQ water, in anhydrous acetone (EMS). The specimens were kept under liquid nitrogen at all times during this process. The freeze-substitution was performed in AFS2 (Leica) with the following program: −90°C for 5-7 hours, 5°C/hour to −20°C, 12 hours at −20°C, and 10°C/hour to 20°C. Following *en bloc* staining with 0.1% uranyl acetate in anhydrous acetone, the samples were infiltrated and embedded into epon and cured for 48 hours in a 60°C oven.

Ultramicrotomy and electron microscopy

Serial 40-nm sections were cut using a microtome (Leica UCT and UC7) and collected onto pioloform-coated (0.7%) single-slot grids. Sections were stained with 2.5% uranyl acetate prior to imaging. For ferritin experiments, sections were not stained after sectioning to improve contrast of ferritin molecules in our images – this, in turn, might have compromised our ability to distinguish clathrin-coated vesicles. Approximately 100-150 synaptic profiles were collected from a single section from each specimen, and the experiments were repeated with second cultures in each case (for detailed n values, see Quantification and Statistical Analysis section). Prior to sectioning, all the samples were blinded to genotypes and treatments to avoid potential bias during imaging. The sample size was chosen based on the previous experiments that allowed us to acquire a sufficiently large set of data for statistical analysis (Watanabe et al., 2013b).

pHluorin imaging

Experiments using synaptophysin-pHluorin imaging were performed on primary continental cultures of hippocampal neurons from littermates. Cultures were infected 24-48 hours after plating and were imaged between DIV13 and 18. Extracellular field stimulation was performed using a perfusion chamber with field stimulation (Warner Instruments). Stimulation protocols were 10 stimuli at 20 Hz or 75 stimuli at 10 Hz for synaptojanin experiments and 10 or 40 stimuli at 20 Hz for endophilin experiments, with each pulse lasting 1 ms. The stimulation chamber was set to deliver 50 mA current for each action potential, the lowest current to achieve stable response to 75 APs (10 Hz) in control cells infected with pHluorin. Before each train of action potentials, baseline images were obtained for 5 s in the absence of stimulation. Images were acquired at a rate of 1 Hz using the Hamamatsu CCD camera with binning of 2, depth of 16 bit, and images 256 × 256 pixels and the CoolLED system with wavelength 470 nm at 60x magnification (NA = 1.2). During imaging experiments, neurons were bathed in extracellular solution containing: 2 mM Ca^{2+} and 4 mM Mg^{2+}, 15 μM bicuculline, 5 μM NBQX, 10 μM AP5. Solutions were delivered through a custom heated flow-pipe (Pyott and Rosenmund, 2002), adjusted for a set point of 35°C, with a range of 34-37°C. Temperatures were also verified by intermittent checks with a temperature probe. Each coverslip was broken with a diamond pencil, and from the pieces generated, fields of view were selected randomly by eye to image. The selection of puncta that were used to analyze pHluorin kinetics is described below.

Electrophysiology

Whole cell patch-clamp recordings in autaptic hippocampal neurons were performed as previously described (Watanabe et al., 2013b). Briefly, extracellular solution contained 140 mM NaCl, 2.4 mM KCl, 10 mM HEPES, 10 mM glucose, 2 mM $CaCl_2$, and 4 mM $MgCl_2$ (pH adjusted to 7.4, and osmolarity adjusted to 300 mOsm). Intracellular solution contained: 136 mM KCl, 17.8 mM HEPES, 1 mM EGTA, 4.6 mM $MgCl_2$, 4 mM Na_2ATP, 0.3 mM Na_2GTP,12 mM creatine phosphate, 50 units/ml creatine-phosphokinase (pH adjusted to 7.4). Solutions were heated to 35°C and applied using the custom-built fast-flow system described above. Borosilicate glass pipettes (Science Products) were used with a resistance of 2-5 MOhm and filled with intracellular solution. Series resistance was compensated 70%, and neurons were stimulated by a 1-ms somatic depolarization to 0 mV from a holding potential of −70 mV. Data were recorded using a Multiclamp 700B amplifier (Molecular Devices) and pClamp 10 software (Molecular Devices), digitized at 10 kHz, low-pass Bessel filtered at 3 kHz, and analyzed with AxoGraph X 1.5.4 (AxoGraph).

QUANTIFICATION AND STATISTICAL ANALYSIS

The experiments were performed in at least two independent cultures unless otherwise noted. Data are pooled and all are included unless otherwise noted. Detailed statistics can be found in Table S1.

Electron microscopy

The total number of synaptic profiles analyzed for these experiments was 10,208. The synaptic profiles were chosen randomly to sample unbiased populations. Active zones were defined as regions juxtaposed to a post-synaptic density. Docked vesicles are defined as those directly in contact with membrane. Morphometry of pits include 'width', which is the opening at the base, 'depth', which is the height from base to top, and diameter, which is measured as the width at half of the depth. The large endocytic vesicles are defined as vesicles larger than ~50 nm by visual inspection and within 50 nm of active zone, measured in ImageJ. Endosomes are defined as membrane-bound organelles that are in the center of the bouton and larger than 100 nm by visual inspection. Vesicular compartments with coated buds were also categorized as endosomes, which appeared frequently in our 3 s time points. Vesicles are scored as clathrin-coated only if distinctive coats were visible which can lead to underscoring. Furthermore, the chance of capturing a coated vesicle in a given synaptic profile is low compared to an endosome due to its size. These factors will lead to an underestimation of the number of coated vesicles observed in profiles. The morphometry was performed blind using custom-written ImageJ macro and MATLAB scripts (S.W. and E.M.J., unpublished data; available upon request).

We used Mann-Whitney U tests or Kruskall-Wallis nonparametric ANOVA for numbers collected in electron microscopy due to the skewed distribution of the data. The skewness was determined using Pearson's skewness test. The confidence level was set at 0.05 in each case. When appropriate, we applied the Bonferroni correction to reduce the chance of obtaining false positive in multiple comparisons on a single dataset. The gray shade in the P value columns suggest the difference observed is statistically significant. The experiments were repeated from at least two independent cultures. All data are pooled and plotted. All collected data were included in the analysis. Numbers are available in the Table S1.

pHluorin imaging

pHluorin images were analyzed in ImageJ, all images for a given field of view were concatenated, background subtracted using "Rolling Ball" background subtraction with radius 50 and corrected for movement using the StackReg plugin (Thévenaz et al., 1998). To identify synapses, circular regions of 2 μm^2 (ROIs) were manually selected from the ΔF between the average baseline (3 images immediately prior to stimulation) and the peak fluorescence following a strong stimulus (300AP at 10 Hz for synaptojanin and 300 AP at 20 Hz for endophilin). By selecting from the peak of an unrelated stack, synapses were chosen on the basis of their response to activity and irrespective of decay kinetics. This set of ROIs was then applied as a mask to the background-subtracted stack, and intensity was measured for each ROI. The trains of interest for each field of view (10 AP, 20 Hz and 75 AP, 10 Hz for

synaptojanin, 40 AP, 20 Hz for endophilin), were then obtained by averaging all ROIs. To compare groups, the raw average intensities for each field of view were baselined to the 3 images immediately preceding the stimulus and normalized to the peak fluorescence following the stimulus. Time constants were obtained by fitting a single exponential in AxoGraph to the decay of each normalized field of view. Percentage of fluorescence recovered at 3 s and 30 s was analyzed using the field of view averages at each time-point after the peak for each field of view. Fields of view are taken from either 1 (*Synj*$^{+/+}$; *Synj1*$^{-/-}$; *Synj1*$^{-/-}$, SYNJ1 (145kD); *Synj1*$^{-/-}$, SYNJ1^{D730A}; *Synj1*$^{-/-}$, SYNJ1^{C383S}; *EndoA2* KO, *EndoA1* KO rescue) or 2 cultures (*EndoA* TKO, *EndoA* DKO, *EndoA1* KO).

We used Kruskall-Wallis nonparametric ANOVA for dataset collected from pHluorin imaging. Dunn's post-test was performed to compare all pairs of columns. Stacks free of motion or focus drift were included in the analysis with the following exclusion criteria: fields of view in which the fluorescence increase and decay pattern was not time-locked to the stimulus, or which did not exhibit exponential decay were excluded from analysis.

DATA AND SOFTWARE AVAILABILITY

The imageJ macros and MATLAB scripts used for the analysis have not been published but will be available to interested individuals if requested. Upon publication, the scripts will be uploaded on our laboratory websites (Watanabe lab, http://www.watanabelab-emanias.com/ ; and Jorgensen Lab, http://jorgensen.biology.utah.edu/). All data produced in this study can be shared upon request.